ANNALS OF GEOPHYSICS, 68, 5, DM560, 2025; doi:10.4401/ag-9322
OPEN ACCESS

DSEBRA – The German Seismological Broadband Array and Its Contribution to AdriaArray – Deployment and Performance

Antje Schlömer[*,1], Joachim Wassermann[1], Marcel Paffrath[2], Kasper D. Fischer[2], Wolfgang Friederich[2], Thomas Meier[3], Dragana Cernih[4], Jovan Dedic[5], Katerina Drogreshka[4], Christos P. Evangelidis[6], George Kaviris[7], Tobias Megies[1], Shemsi Mustafa[8], Jasmina Najdovska[4], Costas Papazachos[9], Besian Rama[10], Arne Schwab[11], Efthimios Sokos[12], Bálint Süle[13], Markus Terpoorten[1], Milena Tomanovic[5], the AdriaArray Seismology Group[14]

(1) Ludwig-Maximilians-Universität München, Department of Earth and Environmental Sciences, Munich, Germany
(2) Institute of Geology, Mineralogy and Geophysics, Ruhr University Bochum, Bochum, Germany
(3) Institute for Geosciences, University Kiel, Kiel, Germany
(4) Ss. Cyril and Methodius University, Faculty of Natural Sciences and Mathematics, Institute of Physics, Seismological Observatory, Kisela Voda, Skopje, Republic of North Macedonia
(5) Institute of Hydrometeorology and Seismology of Montenegro, Podgorica, Montenegro
(6) Institute of Geodynamics, National Observatory of Athens, Athens, Greece
(7) Section Geophysics-Geothermics, Department of Geology and Geoenvironment, National and Kapodistrian University of Athens, Athens, Greece
(8) Geological Survey of Kosovo, Ministry of Economy, Toskan, Prishtina, Kosovo
(9) Geophysical Laboratory, Aristotle University of Thessaloniki, Greece
(10) Polytechnic University of Tirana, Institute of GeoSciences, Department of Seismology, Tirana, Albania
(11) Schwab Research Technology, Steuben-Allee 29, Germany
(12) Department of Geology, Seismological Laboratory, University of Patras, Patras, Greece
(13) Kövesligethy Radó Seismological Observatory, HUN-REN Institute of Earth Physics and Space Science, Budapest, Hungary
(14) List of AdriaArray Seismology Group participants can be found in Kolínský et al. (2025a)

Article history: received February 28, 2025; accepted September 30, 2025

Abstract

The German Seismological Broadband Array (DSEBRA) comprises 100 mobile seismological stations, which are currently contributing to the multidisciplinary international AdriaArray project, launched in 2022 to comprehensively study the Adriatic plate and its surrounding regions. The data collected in this project enable detailed monitoring of seismic activity and imaging of the crustal and upper mantle structures in the Central Mediterranean. DSEBRA stations are deployed across a wide range of geographical locations, including the Alpine foreland of Germany and Austria, the high Alps of Austria, the Pannonian Basin in Hungary, the southern Dinarides in Montenegro, Kosovo, and Albania, North Macedonia, as well as the mainland of Greece. Equipped with state-of-the-art technology and featuring innovative station design and remote monitoring capabilities, these stations enable the acquisition of high-quality data in near real-time, which is essential for early warning systems in this seismically active region. In this study, the noise characteristics of the stations are analyzed in both the frequency and time domains, revealing significant variations

that can be attributed to differences in geographical and geological settings, as well as levels of urbanization. In the frequency range of the secondary microseisms, a split in the double frequency peak is observed at the Balkan stations. This split is attributed to the simultaneous activation of two distinct source regions in the surrounding oceans. This article provides an overview of the distribution and performance of DSEBRA stations within the AdriaArray project. The contribution of DSEBRA to AdriaArray underscores the importance of well-equipped station pools and international collaboration in achieving the scientific objectives of large-scale seismic networks.

Keywords: Large seismic network; Technical equipment; Seismic noise level; Adriatic plate; Balkans

1. Introduction

The development of large-scale seismic networks has significantly enhanced our ability to investigate complex geophysical phenomena, including tectonic activity, earthquake source dynamics, and subsurface structure imaging. In Europe, these networks have been particularly impactful due to the continent's diverse tectonic settings, such as the Alpine orogeny, Mediterranean subduction zones, and cratonic interiors. One of the most productive recent European seismic initiatives was the AlpArray Seismic Network (AASN; Hetényi et al., 2018), a collaborative effort involving 36 institutes from 11 countries. Approximately 280 temporary and 350 permanent seismic stations were deployed across the Alpine mountain range and its forelands. The high-resolution data collected by this seismological network and also by its complementary networks (e.g., SWATH-D; Heit et al., 2021; PACASE; Schlömer et al., 2024), enabled precise characterization of seismic sources, wavefield propagation, and subsurface imaging of the Alpine orogeny. These efforts culminated in over 100 scientific publications (https://alparray.ethz.ch/en/outreach/publications/).

Following the end of AlpArray in 2019, the concept of an even larger network to cover the entire Adriatic plate and its surroundings emerged. This vision was realized with the launch of AdriaArray in 2022 (Kolínský et al., 2025a), a major multidisciplinary international project, which is one of the largest passive seismic experiments ever conducted in Europe, both in scale and in scientific scope. Designed to investigate the complex tectonics and geodynamics of the Adriatic microplate and its surroundings, the project brings together 64 institutions from 30 countries. The backbone network comprises the already existing 1092 permanent broadband stations, including about 100 stations that were not connected to EIDA before, and 436 temporary broadband stations (Fig. 1a). AdriaArray aims to significantly advance our understanding of the geodynamics, active tectonics, and seismic hazards of the central Mediterranean region, with a focus on the Adriatic microplate and its interactions with surrounding plates. Through high-resolution imaging of the crust and upper mantle structure, the project seeks to resolve key questions about lithospheric deformation, subduction processes, and the driving forces behind regional tectonics. The dense network of permanent and temporary broadband seismic stations enables to collect critical data for earthquake monitoring and seismic hazard in this densely populated area.

Given the challenges of securing common funding for large-scale seismic networks, the creation of networks of such dimensions relies heavily on intense collaboration among participating partners and the availability of well-equipped individual station pools. The German Seismological Broadband Array (Deutsches Seismologisches Breitband Array [DSEBRA]) consists of 100 mobile seismological stations and was acquired within the framework of the German Priority Program "Mountain Building Processes in 4D" (SPP-2017 MB-4D) in 2017 to initially contribute to the European AlpArray Seismic Network (AASN: 2016-2019; Hetényi et al., 2018) and later to join other European and international projects. Within the AASN, DSEBRA stations were deployed in the Alpine foreland and the Molasse Basin of Germany and Austria, as well as in the high Alps of Austria (Schlömer et al., 2022a). Additionally, 10 stations extended the complementary AlpArray experiment SWATH-D (Heit et al., 2021; network ZS; Heit et al., 2017) eastward in Austria. Five selected stations of this network continued to operate in Austria, and Italy after the end of SWATH-D. Furthermore, 11 DSEBRA stations were redeployed at former AlpArray locations in Hungary where stations had previously been dismantled, and four stations densified the local network in the eastern region of the country (Schlömer et al., 2022a).

With the end of AlpArray in 2019, unresolved questions regarding the eastern part of the AASN, including the underlying structure of the Eastern Alps, the Western Carpathians, and the Pannonian Basin, led to the formation of the Pannonian-Carpathian-Alpine Seismic Experiment (PACASE: 2019-2022; Schlömer et al., 2024). This collaboration involved 13 European institutes from seven countries, with DSEBRA stations continuing to operate at the former AASN sites using residual project funding. By spring 2022, 60 DSEBRA stations in Germany, Austria and Italy were dismantled and prepared for deployment within the AdriaArray network.

This article provides a detailed description of the DSEBRA's deployment within AdriaArray, including the spatial distribution of stations, noise characteristics in the frequency and time domains, and innovations in station design and remote monitoring technology.

2. Deployment

With the beginning of AdriaArray in 2022, the funding for the deployment and operation of 60 DSEBRA stations was secured by the Deutsche Forschungsgemeinschaft (DFG). The financial resources were divided between Ruhr University Bochum (RUB) to deploy 40 stations in Greece and North Macedonia, and Ludwig-Maximilians-Universität München (LMU) to deploy 19 stations in Kosovo, Montenegro, and Albania. 37 DSEBRA stations kept their former PACASE locations in Austria, Germany, and Hungary. The deployment of these stations was financed by Christian-Albrechts-Universität zu Kiel (CAU) and maintained by LMU and the Hungarian colleagues (Süle et al., 2025). The locations and instrumentation of all stations are provided in Table 1 of the Supplementary Material of this article.

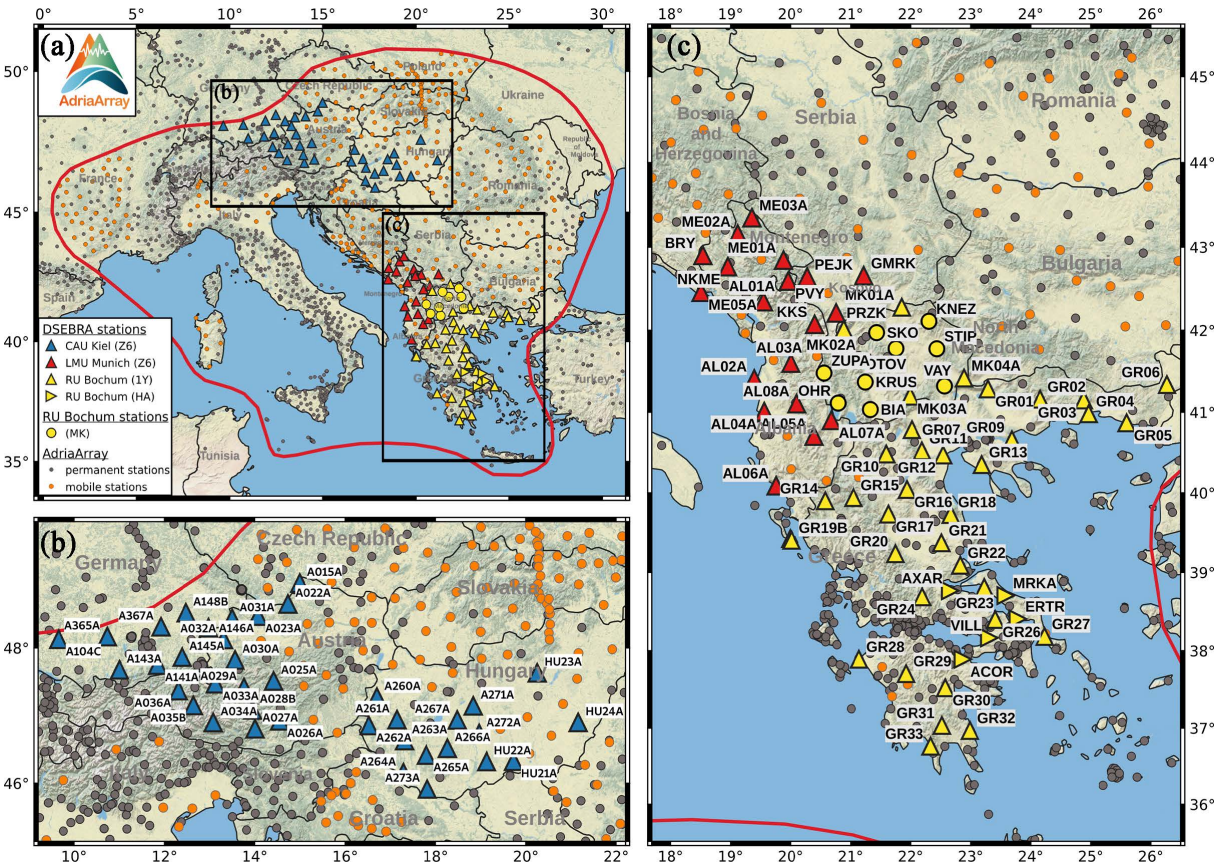

Figure 1. (a) Distribution of DSEBRA and 9 RUB stations within the AdriaArray network (red frame). The map legend indicates the station affiliations along with their corresponding network codes in brackets. (b) CAU stations in Germany, Austria, and Hungary. (c) LMU stations in Montenegro, Albania, and Kosovo, as well as RUB stations in North Macedonia and Greece. In the background, permanent (gray) and temporary (orange) broadband stations with a corner period above 30 Hz are shown.

2.1 Stations in Germany, Austria, and Hungary

With the launch of AdriaArray in 2022, 37 DSEBRA stations were transferred from the PACASE network (network code ZJ; Hetényi et al., 2019) to the AdriaArray network (network code at LMU: Z6; Schlömer et al., 2022b) on 6 December 2022 by keeping their former locations. One station in Austria (A032A) and one in Germany (A367A) had to be dismantled in August 2023 due to construction work at the locations. Currently, 13 stations are installed in Austria, seven in Germany, and 15 in Hungary (Fig. 1; blue triangles). As described by Schlömer et al. (2022a), most of these seismometers are wrapped in cotton wool and covered with buckets to shield them from environmental influences and daily temperature fluctuations. At station A037A, a noticeably quiet site in the high Austrian Alps, the seismometer is installed on a gabbro plate and sealed almost airtight with a pot and rubber rings. At station A029A without a firm foundation, the seismometer is directly buried in the soil, while at A113B, it is also buried in the soil but placed on an underlying flagstone. In the past, all these seismometers were aligned using a gyrocompass (iXBlue Quadrans) to ensure precise north orientation with an accuracy better than 0.23° (Schlömer et al., 2022a). The housing of the stations as well as the characteristics of the basements at the sites are described in Table 1 of the Supplementary Material. Stations oriented with a gyrocompass are also marked.

2.2 Stations in Albania, Montenegro, and Kosovo

During the preparation of DSEBRA stations for their deployment within the AdriaArray project, we benefited from the fact that all of each station's equipment (except for the shielding material) was optimized to fit into a single, stackable box (Fig. 2a and 3a). This significantly facilitated the transportation of the stations to their designated locations.

For the transport to non-European Union (EU) countries such as Albania, Montenegro, and Kosovo, an international logistics company was commissioned to manage the transportation and customs procedures. Within two weeks, 19 DSEBRA stations were delivered to the respective institutes in these countries. A technician from LMU brought the shielding materials and tools and installed the stations in collaboration with local colleagues (Fig. 1; red triangles).

In Montenegro, sites under constant surveillance were selected to prevent sabotage and theft. Thus, government institutions, such as meteorological stations and radio towers, were preferred. In Albania, some non-magnetic containers (Fig. 2b) were used, where other geophysical instruments, such as GNSS (Global Navigation Satellite System) sensors, were already installed. The advantage of these sites is that they provide both a solid concrete foundation for the placement of the seismometer (Fig. 2c) and a power source. However, the disadvantage is the high noise levels due to the nearby machinery, as well as the presence of personnel and animals guarding the sites. In Kosovo, although the three stations are fenced, they are not under continuous surveillance.

The most significant challenges during installation occurred in Kosovo and Albania, where electrical infrastructure is often not conforming to European standards, and characterized by strong voltage fluctuations between 170 V and 230 V. Over the past two years, four chargers had to be replaced in these countries as they were not designed to manage such extreme voltage variations. The delivery of replacement parts from Germany worked smoothly within two weeks.

Almost all seismometers were first wrapped in polishing wool, then covered with a bucket and finally with a rescue blanket (Fig. 2c). At station PVY (Montenegro), the seismometer is directly buried in the soil (Fig. 2d). To prevent damage from rodents and marten bites, the external cables of the stations in Albania, Montenegro and Kosovo were laid in flexible conduits.

Due to EU dual-use regulation, we are not permitted to import the gyrocompass into non-EU countries. Since no equivalent device was available on-site, all 19 stations were oriented northward using a magnetic compass.

Local SIM (Subscriber Identity Module) cards were acquired for the routers, as the use of German SIM cards in these non-EU countries would have been extremely expensive. The router initiates a virtual private network (VPN) connection to the institute to transmit the data. However, mobile data connections in Kosovo and Albania frequently drop at irregular intervals. In most cases, the connection automatically reestablishes, and small amounts of data are subsequently updated via the SeedLink connection, preventing significant data gaps (see Chapter 4).

In conclusion, we were warmly welcomed by the local population, who were very friendly and helpful. The installation process, conducted in collaboration with local colleagues, proceeded smoothly.

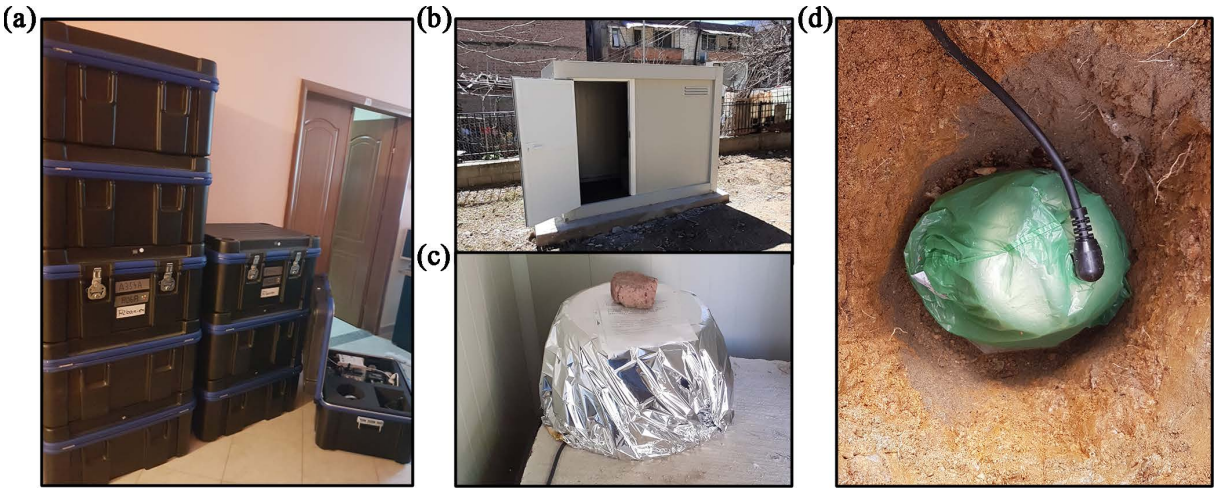

Figure 2. (a) Station equipment optimized to fit into a single, stackable box. (b) A non-magnetic container of station AL05A in Albania with a seismometer installed on a solid decoupled foundation, wrapped with polishing wool and a rescue blanket (c). (d) Seismometer buried in the soil at station PVY in Montenegro.

2.3 Stations in Greece and North Macedonia

The equipment for Greece was shipped in two batches to the National Observatory of Athens (NOA) and the Seismological Observatory of the Aristotle University of Thessaloniki (AUTh) in September 2022. Both batches consisted of 19 fully equipped seismic stations from the DSEBRA pool in single stackable boxes. All 38 instruments were set up by up to five field teams within ten days at pre-scouted sites by local teams at NOA, University of Patras (UPAT), National Kapodistrian University of Athens (NKUA), and AUTh. Each field team included at least one member from RUB and a person from Greece for communication with local people. Starting at NOA in Athens, two alternating teams (RUB-NOA, RUB-UPAT, RUB-NKUA) set up 18 stations in the southern part of Greece. Another 18 stations in the northern part were set up by three teams based at AUTh. Two sets of stations were not set up directly but were prepared for deployment at two other sites which were not ready for use in fall 2022. The equipment from these two remaining boxes has been partially used as spare parts later, and the prepared sites were later set up with different hardware from NOA or AUTh.

Most of the sites in Greece are located inside public buildings, churches, monasteries, or private homes. Thus, these stations are connected to the normal 230V power grid. GR33 is located in an open field vault and powered with solar panels. Details are described below. All stations use a mobile router with SIM cards from WhereverSIM GmbH (Hamburg). These SIM cards are provided by Post Luxembourg without roaming limits. The data volume is pooled for all stations with a data limit of 1.5 GB per station per month. The network code for the temporary deployments in Greece and North Macedonia is 1Y (Friederich et al., 2022). Existing permanent seismic stations with short-period sensors re-equipped with broadband DSEBRA sensors maintain their station names and network codes HA (University of Athens, 2008) and MK (Seismological Observatory at the Faculty of Natural Sciences and Mathematics, Ss. Cyril and Methodius University, Skopje, Republic of Macedonia, 1966).

The 13 stations deployed in North Macedonia were shipped in one batch by a direct transport from RUB to the Ss. Cyril and Methodius University of Skopje in March 2023. Subsequently, the stations were deployed at the end of March by two field teams consisting of one PhD student from Bochum and at least one Macedonian colleague. Out of the 13 deployed stations, only four are part of the DSEBRA pool and were deployed in the newly scouted locations MK01-04 of the temporary network 1Y.

Equipment for the remaining nine stations was assembled from the existing stock at RUB, including five Streckeisen STS2 seismometers and four Güralp CMG-3ESPC 120s seismometers. For good compatibility with the remaining pool, all nine stations were also equipped with Trillium Centaur dataloggers, five of them originating from the RUB stock and four borrowed from the Goethe Universität Frankfurt. Those stations were deployed to upgrade existing monitoring sites of the Seismological network of the Republic of North Macedonia (MK) with broadband stations or to reactivate formerly active sites. The seismometers at the National Observatory

in Skopje (SKO), Ohrid (OHR) and Valandovo (VAY) are installed on concrete foundations with direct contact with the bedrock, which were specifically designed for seismometer operation. The remaining stations are mainly installed in the lowest level of public buildings that were scouted during the field days to have a sufficiently low noise level and good bedrock connection.

The stations in North Macedonia use SIM cards from Makedonski Telekom. The routers in Greece and North Macedonia connect to the servers at RUB in Bochum (Germany) via an OpenVPN connection to reduce costs for static IP (Internet Protocol) SIM cards and increase digital security. Data is transferred using the SeedLink protocol.

All seismometers installed by RUB are shielded against ambient temperature changes and air circulation with shielding made of foam and rescue blankets (Fig. 3b, c).

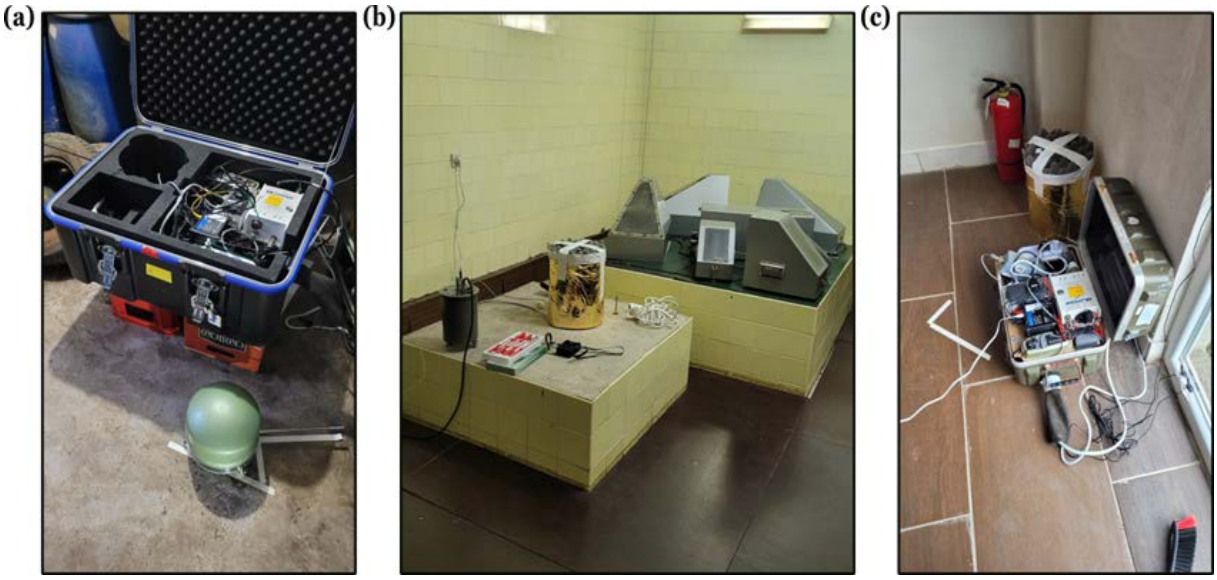

Figure 3. Different examples of station installations in North Macedonia. (a) An STS-2 seismometer with the equipment stored in a box similar to the DSEBRA boxes. (b) A shielded Güralp seismometer on a dedicated concrete base for seismometers at the observatory in Skopje (similar basement at MK.OHR and MK.VAY). (c) Small-scale RUB equipment box for a Güralp seismometer with a shielded seismometer at station MK.ZUPA.

3. Technical Station Design and its Monitoring

The DSEBRA stations are equipped with a three-channel 24-bit data logger (Nanometrics Centaur) and a broadband seismometer (Nanometrics Trillium Horizon, 120 s). A Global Positioning System (GPS) antenna (GA-88P) ensures accurate timing and location data, while a mobile router (Teltonika RUT955) equipped with a 4G Long-Term Evolution (LTE) antenna enables near real-time data transmission (delay <3 s) to either LMU or RUB. Five stations (A015A, A029A, A034A, AL03A, GR33) are powered by solar energy. These stations use two 6 A solar panels (Kyocera KT145-3UC), connected to a solar charger (SunSaver 20L), which regulates the power for two batteries (Yuasa, 12 V, 65 Ah). At all other stations, a battery charger (CTEK MXS 5.0) is connected to the local power grid and charges a 12 V 38 Ah battery (Yuasa NP38) to supply the data logger and seismometer. Due to the high power consumption of the router (~7 W), it was decoupled from the battery and also connected to the local power grid. In case of a power failure, the battery can power the data logger and seismometer for approximately two weeks, providing sufficient time for maintenance. Without this setup, the battery would last less than two days, which is often insufficient to plan and carry out a service intervention.

Nine stations in North Macedonia belong to the mobile pool of RUB. In addition to the Centaur data logger these stations are equipped with either a Streckeisen (STS-2, 120 s) or an Güralp Seismometer (CMG-3ESP, 120 s). For more information about the instrumental configuration of all DSEBRA and RUB stations, see Table 1 in the Supplementary Material of this article. A detailed description of the DSEBRA equipment is provided by Schlömer et al. (2022a).

Both the Centaur and router web interfaces can be accessed via a mobile connection, enabling remote parameter changes. If a working radio link is available, certain commands and status queries can also be sent and received via Short Message Service (SMS), even without an active mobile data connection. When a command is sent, the router responds by confirming its operational status and providing information on the mobile connection status. If no mobile connection is detected, a reboot of the mobile connection or a router restart via SMS may resolve the issue.

However, during the initial deployment of DSEBRA in the AlpArray project, several technical issues were identified:

a. No Remote Access:

Initially, the router was decoupled from the battery to conserve power. However, when no data was received and access to the Centaur and router was not possible via a mobile connection, or the router via SMS, we could not determine whether the issue was a router power failure or a local grid outage.

b. Voltage Drop or Overvoltage:

The charger identifies the battery status and adjusts the charging cycle accordingly. In case of overheating or an error, the charger requires a manual restart (power off/on). Many service interventions to remote locations were made solely to perform this simple reset.

c. Overheating of Battery:

The Centaur's State of Health (SOH) channel only tracked the temperature of the data logger, leaving the internal temperature of the equipment box and its additional components unmonitored. As a result, critical issues like battery overheating could potentially remain undetected.

To address these issues and to avoid unnecessary maintenance trips caused by minor technical problems, a remote monitoring system called PowBox (Fig. 4) was developed by LMU in collaboration with Schwab Research Technology. This device monitors the SOH of the technical equipment, even during power outages, and can remotely control and switch specific devices. At RUB, a Python-based software tool called survBot was developed to analyze the SOH channels of the PowBox and data logger, displaying the information in a graphical interface (Fig. 5) and sending problem notifications via email.

3.1 PowBox

The PowBox is designed to monitor and control devices at a DSEBRA station that cannot be managed via the Centaur or router interfaces. To achieve this, all devices are now connected to the PowBox, including the router, which was originally decoupled from the battery in the initial setup without a PowBox. A circuit diagram of the PowBox is shown in Fig. A1 of Appendix A. All control functions are aiming to guarantee the operation of the seismometer and data logger as long as possible while informing the maintaining institute about any failure. The Centaur's three external SOH channels are used to transmit device status every 30 seconds. Predefined voltage ranges between 0 and 5 V indicate different device statuses. SurvBot continuously queries these values for reporting at the maintaining institutes (see Section 3.2). In the event of a failure, this system enables fast, targeted action, preventing long data gaps. The key functions of the PowBox include:

a. Monitoring the 230V Supply Voltage:

The PowBox monitors the local power grid. In case of a power failure, it waits 20 minutes before switching off the router. This delay provides time for power to return and transmit the status via the SOH2 channel using the still-active mobile connection.

b. Monitoring the Battery and Charger:

The PowBox monitors the 12 V input to the data logger. If the voltage exceeds 12 V, the battery charger is immediately switched off to prevent battery damage. After three minutes, the charger is switched back on, and the voltage is rechecked. If the issue persists after three attempts, the charger remains off until manually reset. In case of an undervoltage of the battery, the PowBox waits for 20 minutes for the voltage to return, transmits the information via SOH and subsequently disconnects the router to save battery.

To prevent potential malfunctions of the charger, which would otherwise require a manual restart, it is automatically restarted every 24 hours with a 3-minute interruption. This routine does not affect the respective charging cycles.

c. Temperature Monitoring:

If the upper temperature limit is exceeded, the PowBox immediately switches off the charger to prevent overheating or battery bursting. After three minutes, the temperature is rechecked, with the cycle repeating three times before a system reset is needed.

d. Router Monitoring:

The PowBox continuously checks the router's status by logging into its console using predefined credentials. If no response is received, the router is switched off for 20 seconds, with the status rechecked after three minutes.

The PowBox can be configured and updated via an RS232 interface (Fig. 4b), where parameters such as router switch-off delay times, charger reset cycles, temperature limits, battery voltage thresholds, and credentials can be adjusted. Firmware updates for the Teltonika router may alter its login behavior, requiring the PowBox firmware to be adjusted accordingly. Three LEDs on the PowBox provide a quick visual status check. If no LEDs are blinking, the system is working correctly. The power consumption of the PowBox varies between a low-power sleep mode (~4 mW) and active mode (~50-120 mW), depending on LED status.

Due to its small size, the PowBox can be easily integrated into the equipment box of a DSEBRA station (Fig. 4a). It has been successfully tested during the PACASE, and currently, 63 DSEBRA stations as well as nine RUB stations are equipped with it (see Table 1 in the Supplementary Material). The PowBox has significantly reduced the number of service interventions caused by minor technical issues, which is a major advantage for installations in remote locations like those in the AdriaArray network. In cases where manual intervention is still required, detailed monitoring helps to identify the faulty component quickly, allowing us and our partners to initiate troubleshooting immediately. The cost of a PowBox is approximately 300 € (depending on order quantity and additional features) and is far more economical than the personnel and travel expenses required for two service interventions.

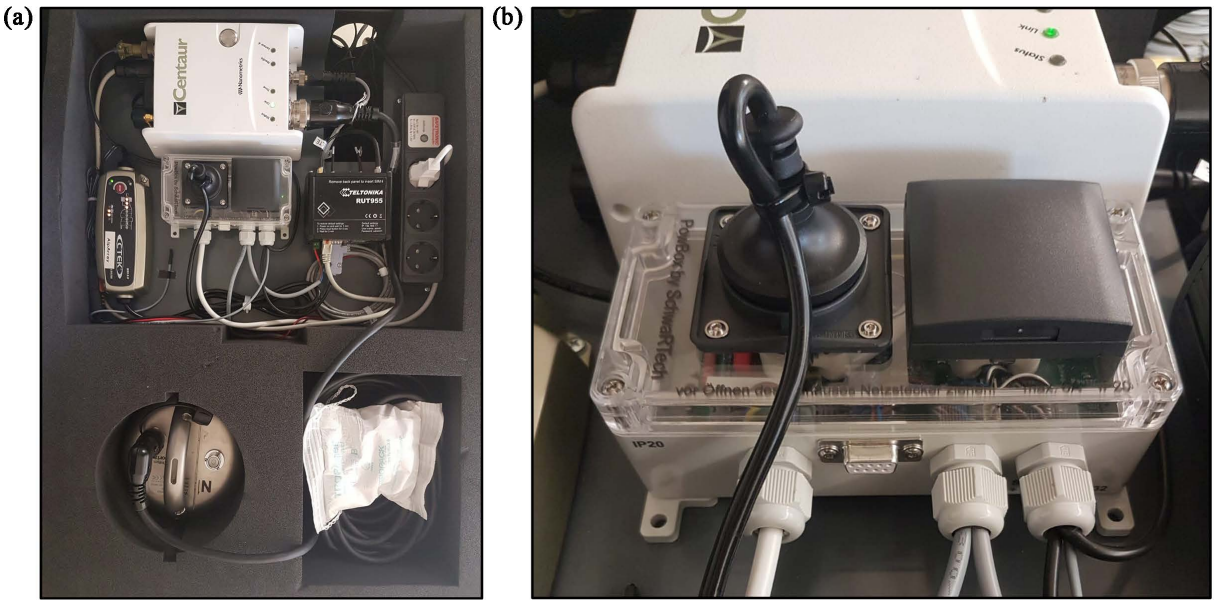

Figure 4. (a) PowBox installed in the equipment box of a DSEBRA station. (b) PowBox in detail.

3.2 survBot

For an easy operator overview of all stations deployed in the field, we developed the software toolkit survBot in Python. It features different methods for the visualization of station problems and for email notification by evaluating critical states in the SOH output of the PowBox devices and additional SOH channels of the Centaur datalogger. It analyzes the latest SOH channel data and creates an overview table that can be displayed as an HTML webpage (Fig. 5), in a graphical user interface or as a simple terminal output.

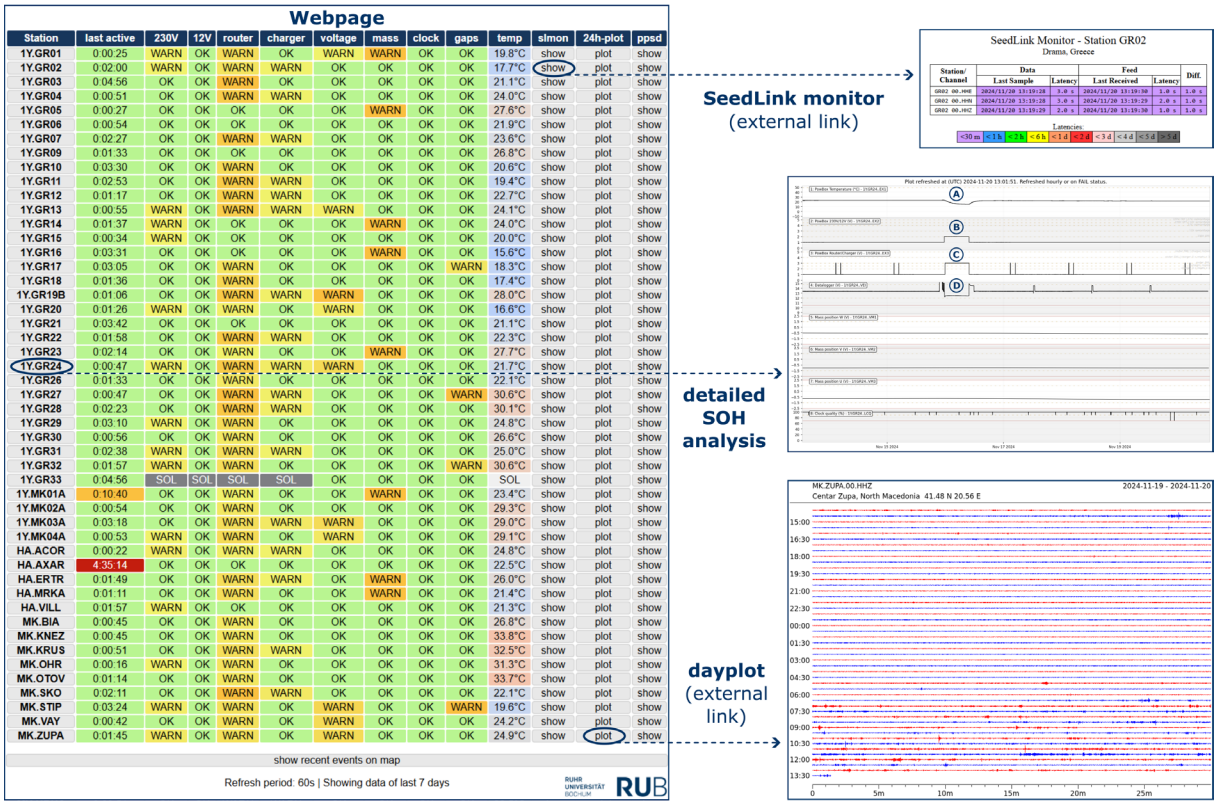

Figure 5. HTML webpage generated by survBot. The rows of the webpage show different stations in the network, while the columns show the activity status, SOH channel analysis, and links to additional websites such as 24-hour or noise plots. Right column: Examples of internal (middle) and external, additional links (top, bottom). The detailed SOH analysis example shows the different output channels of the PowBox after a 230 V power outage. The temperature decreases (A) since the charger does not generate any more heat. The 230 V/12 V channel (B) reports 2V (230 V off). The router status (C) reports a router fail-state 20 minutes after the power loss since the router was switched off. The datalogger voltage channel (D) logs the rapid voltage decrease in the first 20 minutes until the router is switched off.

The software toolkit is meant to run as an addition to data archiving software like SeisComP or Antelope. It evaluates the latest data gathered in a local SDS (SeisComP Data Structure) database in near real-time. Within a user-specified time window of the recent hours/days, all information from the three PowBox SOH channels is read, preprocessed, and the different error states described above are categorized and counted. Additionally, the voltage, mass, and clock channels of the Centaur datalogger are evaluated. Past error states are classified as warnings, whilst present error states are classified as failures (Fig. 5; left). Missing activity (no data) is also categorized as an active failure state. After a user-defined time threshold, active fail states are reported via email to specified persons who are entered in a mailing list as responsible for the corresponding station. For each station, detailed trace plots of the evaluated SOH channels within the read time window are generated regularly (HTML link, Fig. 5; right) or on demand (GUI: Graphical User Interface).

Out of the different visualization options, it has emerged that the HTML webpage is the most frequently used choice in daily practice. Although it lacks some features of the GUI, such as interactive visualization of SOH channel plots, it is – in combination with a web server – simple to access from everywhere and for everyone, i.e., from cooperating institutions worldwide and in the field. In addition, the HTML module enables simple modular expansion of the generated website, by specifying further columns in the parameter file, e.g. with additional links for each station to observatory specific monitoring pages such as data availability/noise plots or 24 h plots (Fig. 5; right), or by general links to station maps etc. (Fig. 5; bottom left).

4. Data Completeness and Access

Figure 6 illustrates the data completeness of all DSEBRA and RUB stations since their installation within AdriaArray. A red line represents any data gap exceeding 90 s, thus, multiple short gaps may appear as a thick red bar. The rounded percentage value displayed for each station reflects its actual data completeness. Due to the efforts to keep the data logger running as long as possible during power failures and due to the use of the PowBox at 63 stations, data completeness reaches more than 99% at most stations. The average data completeness across all stations is 97.2%.

The uniform station instrumentation significantly simplifies the metadata maintenance. Minor errors that had slipped in despite all efforts were identified during a comprehensive check of all AdriaArray metadata (Kolínský et al., 2025b, submitted) and promptly corrected.

Data and metadata from the 96 DSEBRA stations and the additional nine RUB stations are accessible in near real-time through the European Integrated Data Archive (EIDA; Strollo et al., 2021) distributed across the two hosting EIDA nodes, LMU[1] and NOA[2]. LMU hosts data for stations operated by CAU in Germany, Austria, and Hungary, as well as for stations operated by LMU in Albania, Kosovo and Montenegro. All stations in Greece and NorthMacedonia managed by RUB are hosted at NOA. Real-time data can be accessed via SeedLink at both nodes, respectively, for members of the AdriaArray group and by registered seismological observatories for monitoring and alerting purposes. The archived data is restricted with a two-year rolling embargo and is accessible only by AdriaArray group members via the Federation of Digital Seismograph Networks (FDSN) web services, using smart clients or the ObsPy routing client from all available EIDA sources. Member access is managed by the Eida Authentication Service, which uses credential entries in a token to ensure cross-node universal access.

1 https://erde.geophysik.uni-munechen.de
2 https://https://eida.gein.noa.gr

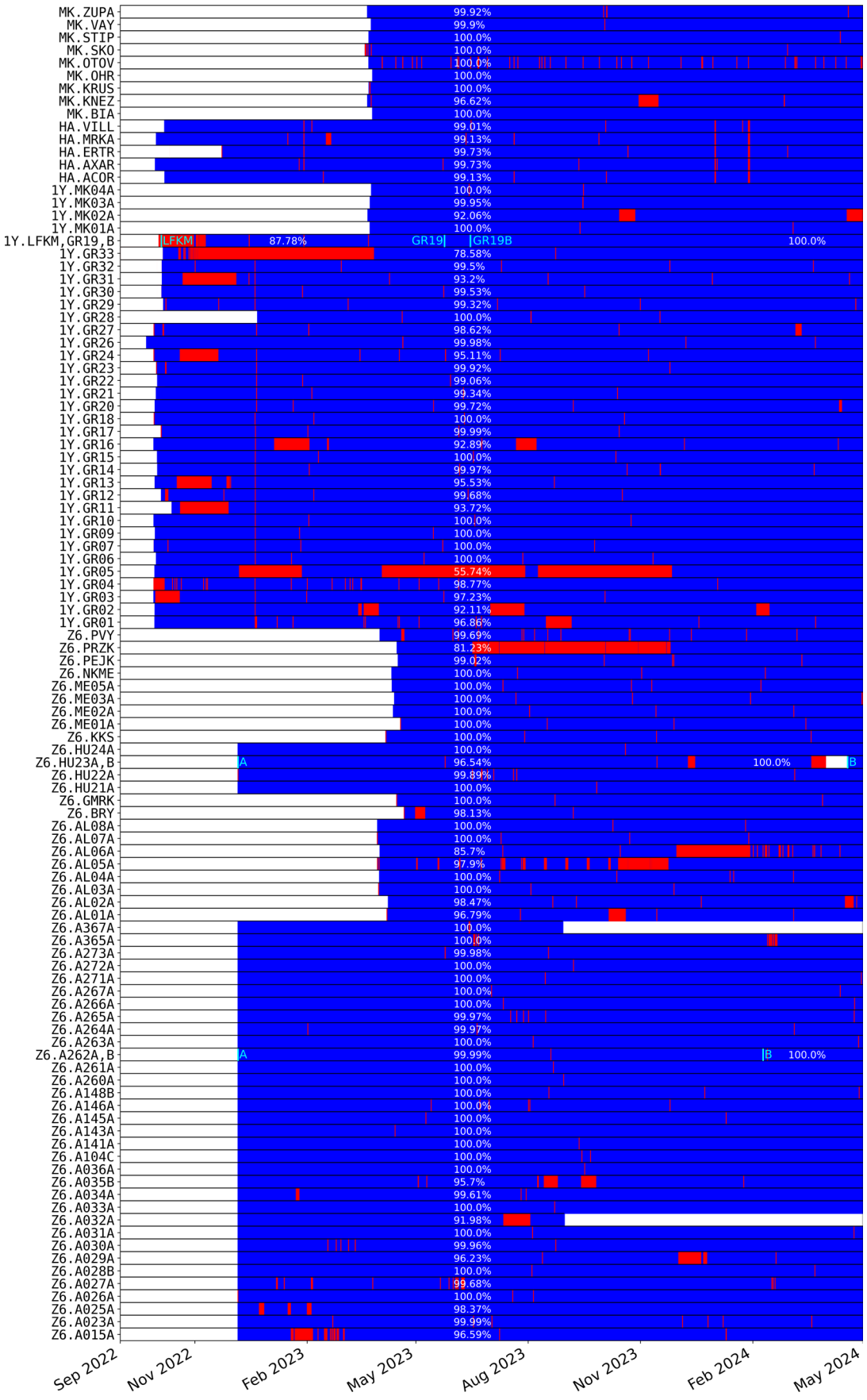

Figure 6. Data completeness of all DSERA and RUB stations. A red line represents any data gap exceeding 90 s, thus, multiple short gaps may appear as a thick red bar. The rounded percentage value displayed for each station reflects its actual data completeness.

5. Noise Analysis in Frequency and Time Domain

The volume of data from large arrays and the rising demands for data quality are increasing continuously, enabled by advancements in computing power. Given the vast data volumes, manual picking for applications such as tomography or receiver function studies is no longer feasible. Consequently, automatic detectors and polarization analyzers have become essential, relying on high-quality data with a robust signal-to-noise ratio.

The uneven spatial and temporal source distribution of microseisms (1-20 s) and microtremors (<1 s), along with variations in their energy levels, can affect seismological processing such as ambient noise tomography and earthquake localization. To provide an overview of noise levels across relevant frequency ranges, we present Probabilistic Power Spectral Density (PPSD) plots. Additionally, we include I95 amplitude values derived from a statistical noise analysis in the time domain, examining the distribution of noise density and its temporal behavior. Data processing was performed using the ObsPy framework (Beyreuther et al., 2010).

5.1 Probabilistic Power Spectral Densities (PPSDs)

PPSDs (McNamara and Buland, 2004) are a useful tool for visualizing seismic noise levels across a broad frequency spectrum. The spectra include cultural noise and diurnal noise at shorter periods (<1 s), tilt- and pressure-induced noise at longer periods (>20 s), and intermediate noise generated by natural sources such as ocean microseisms.

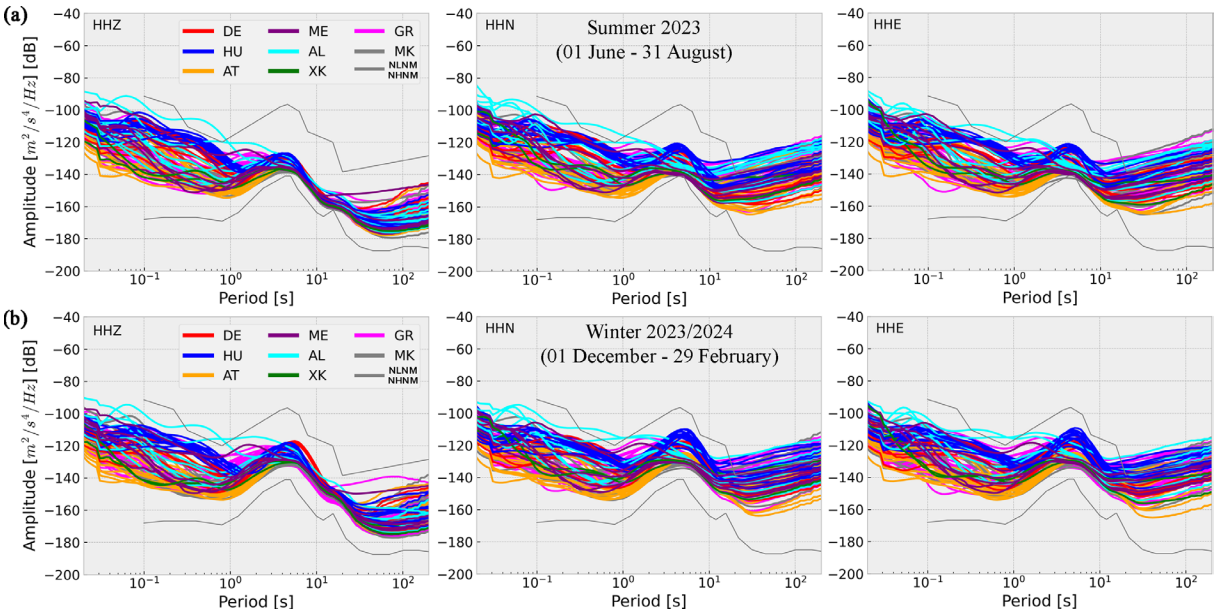

Figure 7. Median curves of Probabilistic Power Spectral Densities (PPSDs) for all DSEBRA and RUB stations for all channels, color coded by country (DE – Germany; HU – Hungary; AT – Austria; ME – Montenegro; AL – Albania; XK – Kosovo; GR – Greece; MK – North Macedonia) for (a) summer (01 June 2023–31 August 2023) and (b) winter (01 December 2023–29 February 2024). Grey lines mark the Peterson New Low/High Noise Model (NLNM; NHNM; Peterson, 1993).

Figure 7 presents the median PPSDs calculated for summer (01 June–31 August 2023) and winter (01 December 2023–29 February 2024) for all components, with color-coded station locations representing different countries. The PPSDs display substantial variations, reflecting differences in station locations and site characteristics: stations cover inland regions (Germany, Austria, Hungary, North Macedonia, and Kosovo) and coastal areas (Greece, Albania, Montenegro), extending from high mountain regions in Austria to lowland basins such as the Molasse Basin in Germany and the Pannonian Basin in Hungary. The seismometers are installed in both urban environments, characterized by fluctuating anthropogenic noise, and remote locations with minimal human activity.

The PPSDs for all stations generally fall below the New High Noise Model (NHNM; Peterson, 1993) for the vertical component and for the horizontal component up to a period of 10 s (Fig. 7). This frequency range is particularly relevant for applications like teleseismic body wave studies and ambient noise tomography. However, at periods around 20 s (and already at 15 s during winter), PPSD levels at many stations exceed the NHNM. This effect, also observed during previous AlpArray and PACASE installations (Schlömer et al., 2022a, 2024), is attributed to insufficient shielding against pressure fluctuations, which can induce long-period horizontal noise by deforming the case of the seismometer (Zürn et al., 2007). While improved shielding could mitigate this noise, logistical and financial constraints make it challenging for temporary deployments.

At periods shorter than 1 s, noise is predominantly anthropogenic, with consistent levels for all components and seasons. Since temporal variations in urban noise are best analyzed in the time domain, this will be addressed in the following chapter.

By focusing on the period range of 1-20 s, which is critical for common seismological applications and the study of microseisms, we classified the noise at all stations into six distinct noise classes, each with unique characteristics (see Fig. B1 in the Appendix B). For an initial approach to station clustering, we combined the mean PPSDs of all three components in a frequency range of 1-20 s and used the Python package SciPy to cluster the waveforms. The PPSD data from six stations were excluded from processing due to missing data (PRZK, GR05, GR19, GR19B) and unusually high temporary noise levels above 10 s (OTOV, AL04A, GR06) within the analyzed time windows, likely caused by transient environmental or anthropogenic sources. All other stations were manually assigned to six distinct clusters. Figure 8 displays the median curves for these six noise clusters on the vertical and north components during the summer (Fig. 8a) and within a winter period (Fig. 8b). Figure 8c provides a map of all stations, indicating their respective noise cluster affiliations.

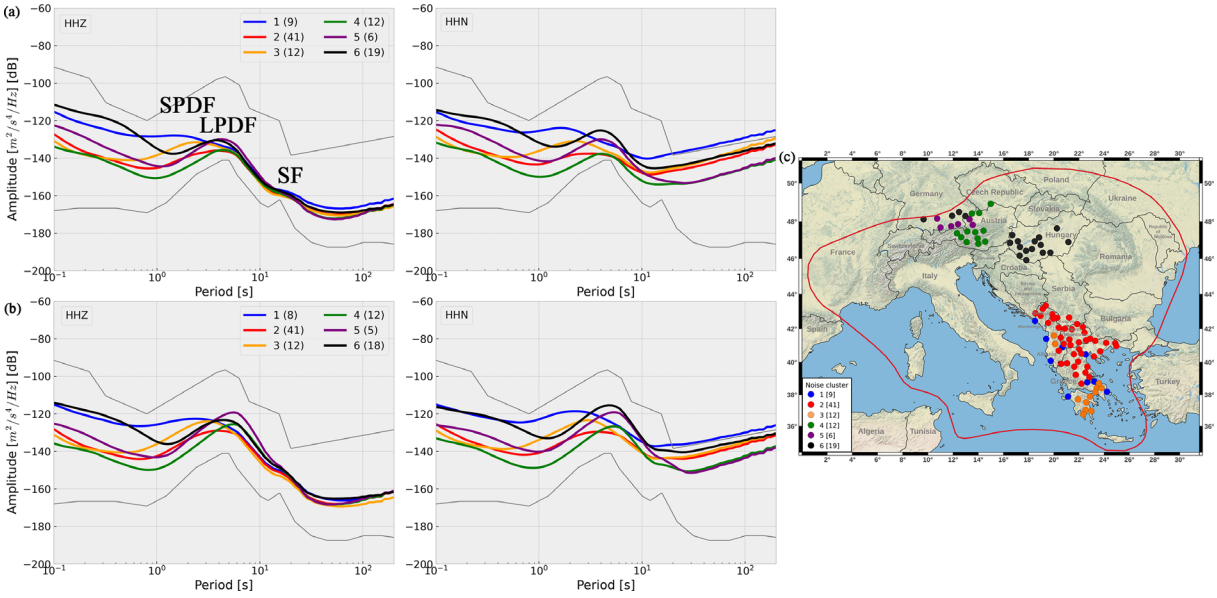

Figure 8. Median curves of all six clusters during (a) the summer season (01 June 2023–31 August 2023) for the vertical and north components and (b) the winter season (01 December 2023–29 February 2024) for the same components. The gray lines represent the Peterson New High/Low Noise Model (Peterson, 1993). SPDF: short-period double frequency; LPDF: long-period double frequency; SF: single frequency; see text for further descriptions. (c) Map showing all stations and their cluster affiliations.

5.1.1 Secondary Ocean Microseisms

The secondary ocean microseisms occur within the frequency range of 1-10 s. Longuet-Higgins (1950) and later Hasselmann (1963) proposed that these microseisms are generated by the superposition of ocean waves traveling in opposite directions, forming standing waves of twice the frequency and therefore termed as double-frequency (DF) peaks. Subsequent research has shown that DF microseisms may also originate near the coast, typically in shallow water

regions (e.g., Bromirski et al., 2005; Koper and Burlacu, 2015; Li et al., 2022; Wiesenberg et al., 2024). In Fig. 8a and b, two distinct peak behaviors can be observed. While stations in central Europe (Fig. 8; green, purple and black) generally follow the New Low Noise Model (NLNM; Peterson, 1993) with the DF peak between 3 to 7 s, the Balkan stations display a double peak pattern during summer (Fig. 8a; blue, red, and orange) at 1.5-3 s and 4-7 s. During winter (Fig. 8b), these stations show a broader bulge between 1.5 and 7 s. The first DF peak at shorter periods is more prominent at coastal and southern Greek stations (Fig. 8a; clusters 1 and 3). Meanwhile, stations in cluster 2 (Fig. 8; red stations), located inland in Greece, North Macedonia, and along the Aegean coast, show slightly elevated energy levels between 4-7 s.

These two noise peaks can be attributed to a split in the DF (e.g., Bromirski et al., 2005, 2013; Li et al., 2022). Bromirski et al. (2005) proposed a short-period double frequency (SPDF) occurring in the 2-5 s range and a long-period double frequency (LPDF) occurring in the 5-12 s range. Since both SPDF and LPDF propagate primarily as Rayleigh waves, their energy attenuates differently. SPDF energy, associated with local wind variability, dissipates more rapidly as it travels inland. This fast attenuation explains why this SPDF is not visible at central European stations and is more prominent at Balkan stations closer to the ocean (clusters 1 and 3). In contrast, stations in inland Greece and along the Aegean coast (cluster 2) display higher energy levels in the LPDF range (4-7 s), which can be assigned to more distant, coastally generated microseisms. Evangelidis and Melis (2012) analyzed ambient noise levels at various stations in Greece, including one station located on the mainland and another station located on an island in the Aegean Sea. Their results revealed noise differences that can be compared to the variations observed between clusters 2 and 3. The authors suggested that stations in southwestern and western Greece are influenced by wave activity originating in the Aegean and Ionian Seas.

Previous studies (Cessaro, 1994; Bromirski et al., 2005) have shown that certain shorelines generate more microseism energy than others. Most of the observed LPDF energy in this case likely originates from the Ionian Sea or even from the North Sea, which are stormier and experience higher wave heights than the closer but calmer Aegean Sea (Caloiero et al., 2022). It has been shown that stations located in Austria and also on the northern Adriatic coast in Italy detect microseism energy generated by the Atlantic Ocean (Retailleau et al., 2017). Consequently, LPDF seismic energy recorded at stations in Central Europe likely originates from the North Sea and Atlantic Ocean rather than the Adriatic Sea.

During winter, SPDF and LPDF amplitudes increase by approximately 10 dB, and their peak periods shift from 2 and 4 s in summer to 3 and 6 s, respectively. Similar seasonal shifts and amplitude increases have been observed at Indian stations during monsoon conditions (Jha et al., 2023), in the North Atlantic (Rykunov, 1967), and also in the Mediterranean Sea (Stutzmann et al., 2009; Borzì et al., 2025). These changes are attributed to increased seismic energy transfer from sea waves to the solid Earth during winter storms, as well as variations in the location of noise sources. The broader frequency extent of peaks in winter and the narrower frequency extent in summer, observed at the Balkan stations, also reflect seasonal variations in ocean wave activity. High winter waves extend SPDF to longer periods, causing it to merge with LPDF signals. A wave height analysis in the Mediterranean Sea (Sartini et al., 2017) reveals maxima southwest of Greece and in the central Aegean Sea (west of cluster 3) during winter, and south of Türkiye and the central Aegean Sea during summer. This observation explains the higher amplitudes of the SPDF peak in cluster 3, as well as its shift to longer periods during winter due to the movement of the dominant noise source to a more distant location.

In cluster 6 (Fig. 8; black), significant amplitude differences (~10 dB) between vertical and horizontal components in the 1-10 s range are observed. These stations, partially located in the Molasse Basin (Germany) and the Pannonian Basin (Hungary), are affected by sedimentary basins that contribute to higher horizontal noise at periods around 5 s (Gráczer et al., 2018; Schlömer et al., 2024). Langston et al. (2009) observed a similar effect in the Mississippi Embayment, where Rayleigh and Love waves generated at the U.S. coast converted into vertically propagating shear energy, which reverberated with sediments. The period of the secondary microseisms at these stations (Fig. 8; cluster 6; black) on the vertical component is 1-2 s lower than similar peaks observed at cluster 4 and 5 stations (Germany and Austria), where only the amplitude of cluster 5 is 10 dB higher. Koper and Burlacu (2015) observed a similar reduction in rift and basin regions of North America and concluded that the geometry of the sedimentary basins enhances spatial resonance effects at shorter-period DF energy.

5.1.2 Primary Ocean Microseisms

Primary microseisms with periods ranging from 10-20 s are typically generated by the interaction of ocean waves with the sea bottom in shallow waters or by surf (e.g., Hasselmann, 1963; Bromirski et al., 2005). These seismic

waves have the same frequency as the ocean waves that generate them and are known as single-frequency (SF) microseisms. All stations display a shallow bulge on the vertical component in this frequency range (Fig. 8; left). Unlike the varying peak periods observed in the DF microseisms, all stations show a consistent peak period in this case. The seasonal variation shows a peak that is more than 10 dB higher in winter compared to summer (Fig. 8b; left). This bulge is only slightly visible on the horizontal component at the quietest stations during winter (Fig. 8b; clusters 2, 3, 4, and 5). Similarly, Ardhuin et al. (2015) identified the dominant feature of primary microseisms in the vertical spectra at stations located in Europe. They suggested that ocean waves traveling perpendicular to shallow-water topography result in a stronger vertical amplitude. However, Gualtieri et al. (2019) argued that assuming the closest coastline as the source of primary microseisms can be misleading. Given that the PPSDs of all stations display a consistent peak behavior, we propose a common dominant source, such as the North Atlantic, as the generation area for primary microseisms observed at all stations. Results revealed by a correlation between high noise levels of Greek stations and strong storms in the North Atlantic (Evangelidis and Melis, 2012) support this assumption.

A detailed, frequency-dependent polarization analysis would be necessary to determine the azimuthal orientation of these sources and to enable precise differentiation of the oceanic regions contributing to these SF and DF peaks.

5.2 I95 Amplitude Values in the Time Domain

To investigate temporal variations in noise, a statistical noise analysis was conducted in the time domain, complementing the frequency-domain investigations described above. While the above approach focuses on identifying specific characteristics of the noise spectrum within narrow frequency ranges, the time domain analysis is particularly useful for estimating bulk noise levels across broader frequency bands, which are commonly used for basic seismogram interpretation. This approach is advantageous for obtaining velocities (µm/s) compared to calculating PPSDs (dB). These velocities can be directly used for setting detection triggers, identifying critical velocity thresholds for signal-to-noise ratio analysis, and examining temporal variations over specific periods. For this purpose, we calculated the I95 amplitude values (Groos and Ritter, 2009), which represent the 95% confidence interval. This threshold indicates the noise levels below which 95% of the data falls in a selected time window. These I95 values are calculated and visualized using the Python toolbox i95_sds, which has been previously demonstrated in Schlömer et al. (2022a, 2024). Now, this toolbox is openly accessible on GitHub (https://github.com/megies/i95_sds) and described in detail in Appendix C. I95 values are computed from data filtered in the frequency ranges 0.1-5 Hz and 1-20 Hz using a sliding 1-hour window, averaged over 30-minute intervals. The toolbox allows for the visualization of results as line or violin plots. Violin plots, which combine features of box plots and kernel density plots, highlight deviations from a Gaussian distribution. By additionally using a line plot, these deviations can be assigned to specific time intervals in which the noise variations occur.

To provide a regional overview of the I95 amplitude values and noise distribution of all DSEBRA and RUB stations, violin plots were created for the German, Austrian, and Hungarian stations (Fig. 9) and separately for the Balkan stations (Fig. 10). The violins are not scaled by size; instead, color indicates the mean I95 amplitude values in µm/s, while the violin shapes reflect differences from a Gaussian-like distribution, either unimodal or multimodal. Each violin spans from the lowest I95 amplitude value recorded at the respective station to the 95th percentile of I95 amplitude values. Significant differences were observed between summer and winter in the 0.1-5 Hz frequency range (Fig. 9a, b and Fig. 10a, b) and between the two frequency ranges during summer (Fig. 9b, c and Fig. 10b, c). These differences are specifically discussed in the following subsections. All other I95 values for both frequency ranges, both seasons, and for all components are presented in Fig. D1 of Appendix D.

5.2.1 Noise Distribution at Stations in Germany, Austria, and Hungary

A comparison of I95 amplitudes in the 0.1-5 Hz range between summer and winter (Fig. 9a, b) reveals significantly higher amplitudes on the horizontal components during winter, particularly at stations located in the Molasse Basin in Germany and the Pannonian Basin in Hungary. In this frequency band, there is a mixture of natural noise sources, such as ocean-generated noise, and anthropogenic noise with the former typically much stronger during the stormy seasons of fall and winter. In winter, ocean-generated noise often dominates this frequency band,

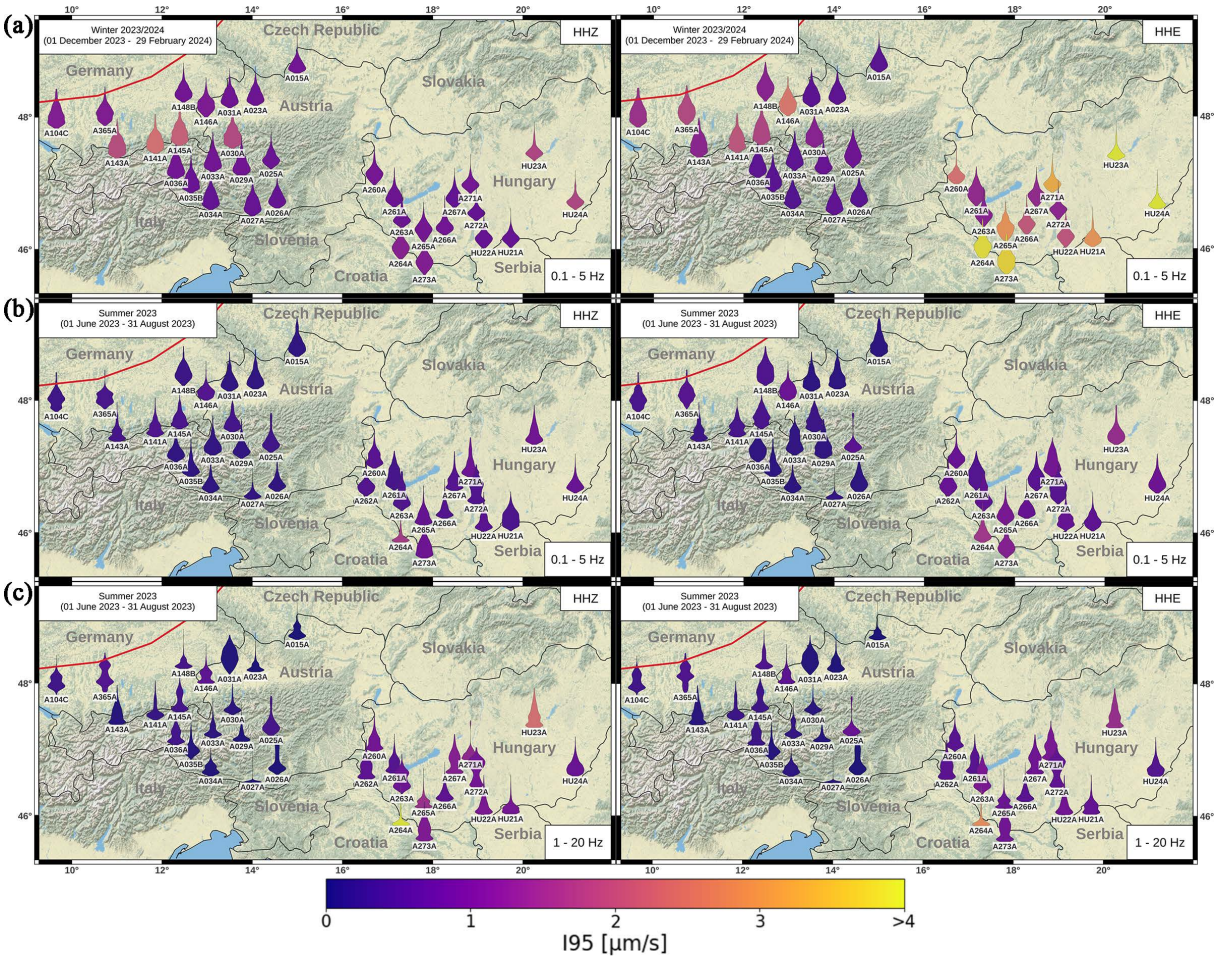

Figure 9. (a) Violin plots of Central Europe stations during winter in the 0.1-5 Hz frequency range and (b) during the summer, showing the vertical (left) and east (right) components. (c) Violin plots during summer in the 1-20 Hz frequency range. The violins are not scaled by size; instead, color indicates the average I95 amplitude values in µm/s, while the violin shapes reflect differences from a Gaussian-like distribution, either unimodal or multimodal. Each violin spans from the lowest I95 amplitude value recorded at the respective station to the 95th percentile of I95 amplitude values.

resulting in predominantly single-mode noise distributions. In contrast, the summer values are comparable for both components in the 1-20 Hz range, which is more influenced by anthropogenic noise sources. This pattern corresponds to the differences identified in cluster 5 of the PPSDs (see Section 5.1), which indicate higher horizontal noise levels at sites situated in sedimentary basins. Several stations in Hungary (e.g., A261A, A267A, A271A, A272A, HU21A and HU23A) show a single-mode noise distribution during winter, associated with higher overall noise levels (Fig. 9a) and a bimodal distribution in summer, when overall noise levels are lower. This pattern may reflect diurnal variations and changes in anthropogenic noise during workweeks (Fig. 9b, c). This behavior is also observed at some Austrian stations on the horizontal component (e.g., A015A, A023A, A031A, A029A; Fig. 9a, b; right). Many Hungarian stations are located in vaulted cellars of small wineries, where the second mode in summer could be attributed to variable noise levels from winemaking activities. Additionally, the violin plots for the two frequency ranges display distinct shapes during summer (Fig. 9b, c; e.g. A015A, HU21A, A260A, and A265A), indicating varying noise characteristics across a broad frequency spectrum.

5.2.2 Noise Distribution at Stations in Montenegro, Albania, Kosovo, North Macedonia, and Greece

The I95 amplitude values of the Balkan stations reveal no significant differences between the vertical and east components in both frequency ranges (Fig. 10; left and right), unlike stations located in the basins. However,

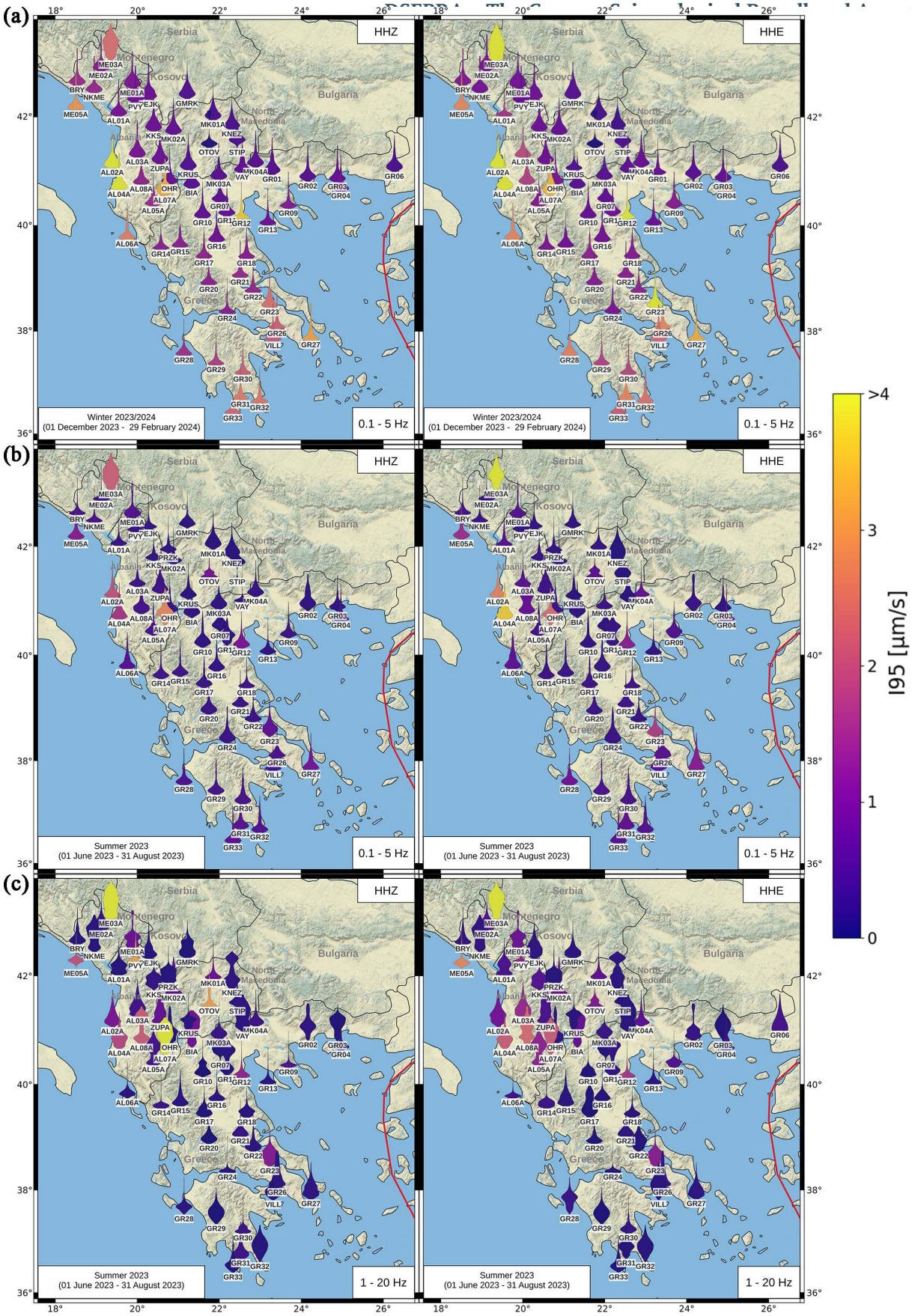

Figure 10. (a) Violin plots for Balkan stations during winter in the 0.1-5 Hz frequency range and (b) during summer, showing the vertical (left) and east (right) components. (c) Violin plots during the summer season in the 1-20 Hz frequency range. The violins are not scaled, therefore the color indicates the average I95 amplitude value, while the shape of the violins reflects the differences from a normal distribution. The violin stretches from the bottom with the lowest I95 amplitude values and ends with the 95th percentile of I95 amplitude values.

I95 amplitudes are considerably higher in the 0.1-5 Hz frequency range during winter than summer for both components (Fig. 10a, b). This increase is especially noticeable at southern and coastal stations along the western Albanian coast and in southern Greece. Here, ocean wave heights and winter storms increase the double-frequency microseismic energy levels during winter (Li et al., 2022). In the 1-20 Hz range, stations in Montenegro, Albania, and North Macedonia show the highest I95 amplitudes during summer (Fig. 10c). This elevated noise is primarily anthropogenic, resulting from constant surveillance of the sites, as discussed in Section 2.2, and traffic from nearby roads.

To further investigate these temporal variations, we analyze the line and violin plots for station ME01A, located in western Montenegro. The analysis focuses on the summer season within the 1-20 Hz frequency range (Fig. 11) for the vertical component. In the violin plot on the right (Fig. 11a), the gray bar inside the violin represents

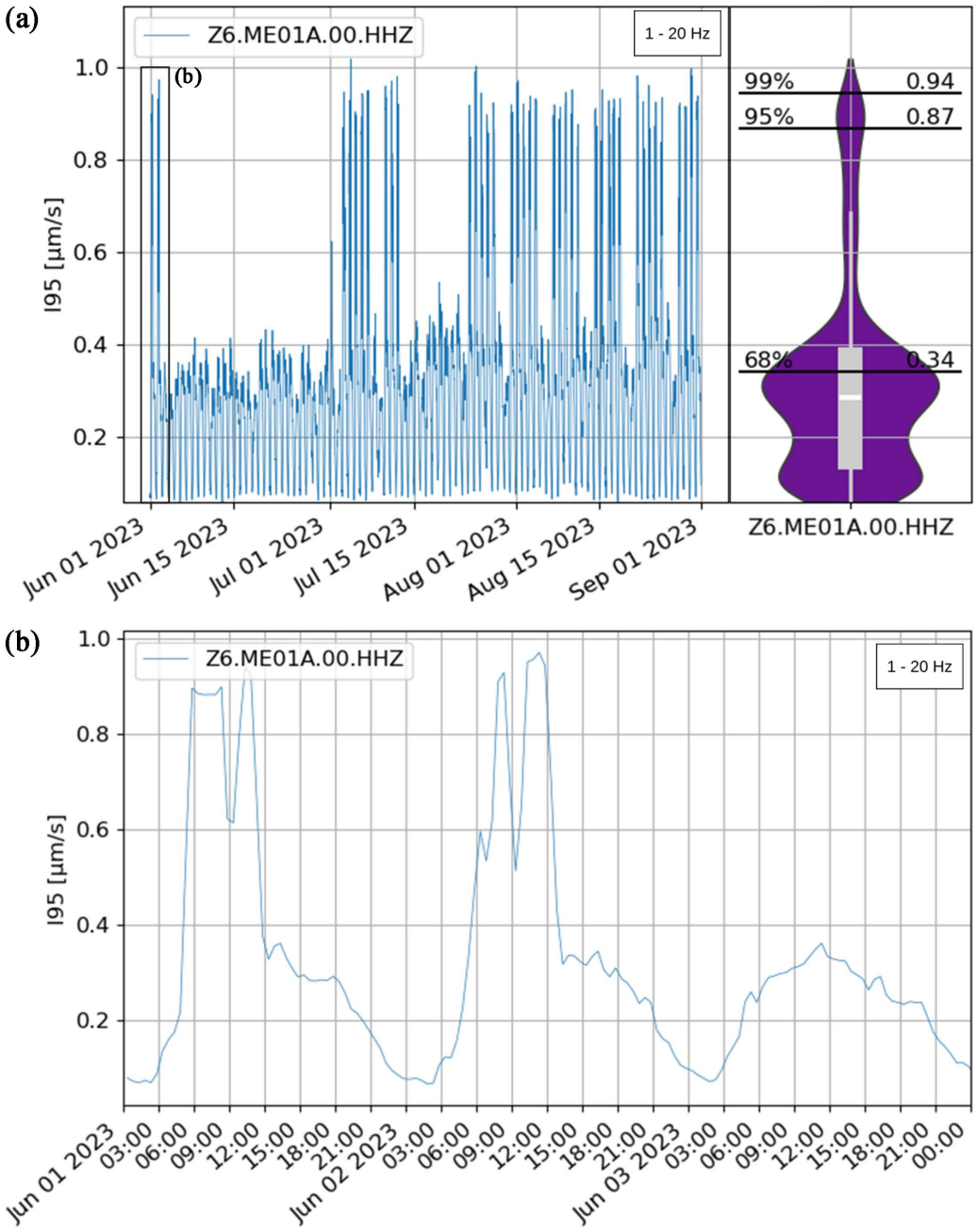

Figure 11. (a) Line plot (left) and violin plot (right) for station ME01A, installed in the basement of a meteorological observatory in Berane, Montenegro, during the summer of 2023. The analysis focuses on the vertical component within the 1-20 Hz frequency range. (b) A three-day line plot (01 June 2023–03 June 2023) for station ME01A, showing the vertical component.

the interquartile range (50% of the data), with the median marked by a white line. Black horizontal lines denote quantiles at 68%, 95% and 99% of the data, alongside their corresponding amplitude values. The horizontal width of the violin represents the full noise distribution, allowing for the identification of multimodal distributions, their amplitudes, and their positions.

The violin plot in Fig. 11a reveals a multimodal noise distribution with two stronger modes below the 68% quantile and a weaker mode between the 95% and 99% quantiles. In the corresponding line plot on the left, a clear day/night periodicity is evident, corresponding to the lowest mode at ~0.08 µm/s for nighttime noise and the second strongest mode at ~0.3 µm/s for normal daytime noise. A weaker mode at ~0.9 µm/s can be associated with higher daytime noise, particularly on some working days.

The seismometer is located in the basement of a meteorological observatory in a small town near a road with through traffic and a small parking area in front. Within a 300 m radius, there is a primary school, a gym, and a hotel. Three modes can be observed in the noise distribution. The lowest mode corresponds to reduced anthropogenic noise during nighttime hours, when the site is unoccupied and traffic and human generated noise is minimal. The strong intermediate mode reflects typical daytime noise levels from surrounding sources, while the highest mode corresponds to increased on-site noise, when staff are present and working on the premises. The observatory staff works daily from 7 AM-2 PM and 7-9 PM (UTC+2), which corresponds to a strong increase in noise at 5 AM (UTC) and a decrease at 12 PM (UTC) in the first two days of a zoomed line plot (Fig. 11b), showing the first three days of June. A working break at 9 AM (UTC) is also detectable. The lower daytime noise on the third day in Fig. 11b is likely due to it being a Saturday, when daytime activities are strongly reduced.

The ratios of the I95 and I68 quantiles serve as indicators of inequality between the highest and lowest values. When many amplitude values exceed the I68 quantile, the noise exhibits high inequality, corresponding to a high I95/I68 ratio ($\gg$2). In this specific time window (Fig. 11a), the daytime noise shows significant inequality (I95/I68 = 2.5), which stretches the violin. The I99/I95 ratio serves as an indicator of outliers: noise with numerous high-amplitude outliers results in a high I99/I95 ratio ($\gg$1.5), whereas fewer outliers correspond to a ratio closer to 1. In this example for station ME01A, the number of outliers is exceedingly small, as indicated by an I99/I95 ratio of 1.08.

To assess the number of outliers and noise inequality at all DSEBRA and RUB stations, all ratios are presented in Fig. D2 and D3 in Appendix D.

6. Impact of DSEBRA Stations

The DSEBRA stations currently form the core of the AdriaArray experiment (Kolínský et al., 2025a) and previously contributed to the AlpArray and PACASE networks (Hetényi et al., 2018; Schlömer et al., 2024). DSEBRA has therefore made a major contribution to the deployment of regional arrays in Europe, resulting in numerous scientific publications, including imaging of seismic wavefields in the Alps (e.g., Kolínský et al., 2019, 2020; Ling et al., 2021; Paffrath et al., 2021a; Tesch et al., 2022; Lu et al., 2022) and in the Adriatic region (Stampa et al., 2025). The main scientific objective of AlpArray and PACASE was passive seismic imaging of the Alpine deep structure to reveal the driving forces of continental collision and mountain building. For example, data of DSEBRA stations have already been used in a number of tomographic (e.g. Lu et al., 2018; 2020; Alder et al., 2021; Paffrath et al., 2021b; Plomerová et al., 2022; Najafabadi et al., 2022; Nouibat et al., 2023; Menichelli et al., 2023; Timkó et al., 2024; Bagagli et al., 2025) and receiver function studies (e.g. Michailos et al., 2022; Kind et al., 2021; 2023; Mroczek et al., 2023; Kalmár et al., 2023; 2025) to image small-scale slab and crustal structures in the Alpine region and its foreland basins. Building on this data potential, we expect a comparable number of scientific outcomes from AdriaArray, particularly in identifying the geodynamic drivers of geohazards, which represent its primary scientific target.

In the framework of AdriaArray, registered seismological observatories can access the real-time data of DSEBRA stations via a SeedLink server for monitoring and alerting purposes. Together with real-time signal processing tools, this enables them to receive and analyze seismic data almost instantaneously, which is crucial for early warning systems in this seismically active, densely populated region.

The DSEBRA stations significantly enhance local and regional catalogs by either filling critical gaps in the seismic coverage or updating sites equipped with short-period seismometers to broadband seismometers. This densification enhances the monitoring capabilities and allows for a better characterization of seismic activity, including more accurate triangulation of earthquake epicenters, and allows the localization of small, previously undetected events.

In Hungary, 15 DSEBRA stations are integrated into the Hungarian National Seismological Network, contributing to approximately one-third of the local network. This integration has significantly enhanced the detection capabilities for seismic events occurring in the Carpathian-Pannonian region (Süle et al., 2025). The catalog shows an increasing trend in the number of detected earthquakes, along with progressively lower detection thresholds and improved accuracy over the last years, demonstrating the benefits of the expanded station network. The detection of the recent Szarvas earthquake swarm in the summer 2023, with the smallest recorded magnitude of 0.8, highlights the network's high detection sensitivity. Additionally, many recent studies have been published utilizing data from the Hungarian network (Süle et al., 2025, and references therein).

In April 2023, nine DSEBRA stations were incorporated into the National and Regional Monitoring Infrastructure of the Albanian Seismic Network. Since then, the AdriaArray network in Albania has recorded more than 13,000 earthquakes, which account for approximately 60% of the total events detected by the Albanian Seismic network (Dushi et al., 2025, submitted). Among these stations, AL05A demonstrated the highest event detection performance (~3,500 events) with various seismic phases. The DSEBRA stations have also enhanced the spatial coverage of real-time moment tensor solutions, enabling the computation of solutions for smaller events and the identification of more localized fault systems. Furthermore, the DSEBRA stations have been integrated into the SHAKEMAP service and serve as a valuable data source for this purpose.

The data recorded by the AdriaArray (1Y) stations, along with those by the Hellenic Unified Seismological Network (HUSN; Evangelidis et al., 2021), played an important role in the detailed monitoring of the earthquake sequences that occurred recently in the vicinity of the Euboea Island (Central Greece). In more detail, the 1Y stations increased the event detections by 31%-47% and enhanced the quality of solutions, due to their proximity to the seismically activated areas on the Euboea Island, as analyzed by Spingos et al. (2024). The most important sequences were the Styra-Zarakes swarm, the Psachna sequence, and the sequences with an Mw = 4.3 event on 04 January 2023 (Markates) and an Mw = 5.0 event on 03 November 2023 (Prokopi). Regarding the Styra-Zarakes swarm, station GR27 (1Y) of the AdriaArray Network was the closest, at distances of 2 km from 10 km to the onshore epicenters and up to 15 km from the offshore ones, playing a major role in the reduction of vertical location uncertainties (Evangelidis and Fountoulakis, 2023; Spingos et al., 2024).

Data from the Styra-Zarakes swarm, recorded by the GR27 station (network 1Y), were also used to investigate seismic anisotropy through shear-wave splitting (Spingos et al., 2024), which was attributed to along-fault fluid processes. An automatic procedure was applied to determine the polarization direction of the fast shear-wave (mean value N68°E) and the time-delay (average value 80 ms). Temporal variations of the splitting parameters were identified and related to outbursts of seismicity.

Additionally, 1Y stations are utilized in the Automatic Moment Tensor Monitoring Service of NOA, which operates using the GISOLA software (Triantafyllis et al., 2021). This service estimates Moment Tensor solutions (MTs) for events with magnitudes greater than approximately 3.6 ML.

Starting in March 2023, a total of 13 seismological stations have been established across North Macedonia, with nine contributed by RUB and four by DSEBRA. The addition of these stations greatly strengthens the continuous monitoring of seismic activity in the region. This expansion is vital not only for enriching and standardizing the earthquake catalog but also for enhancing the accuracy of earthquake location data. Furthermore, the increased number of stations plays a crucial role in determining earthquake mechanisms (FPS), offering valuable insights into the underlying causes of seismic events.

In summary, the DSEBRA stations support AdriaArray by increasing seismic station density, improving data quality, and enabling more precise imaging of the Earth's structure in the Balkan and Adriatic regions. The data from these stations enhances the ability to study earthquake processes, plate interactions, and geodynamics in one of Europe's most tectonically complex areas.

7. Conclusions

96 DSEBRA and nine RUB stations were deployed in Germany, Austria, Hungary, Montenegro, Kosovo, Albania, North Macedonia, and Greece to contribute to the backbone network of the international, multidisciplinary AdriaArray project. This project spans the entire Adriatic plate and its surrounding regions.

The stations are equipped with state-of-the-art technical instruments, delivering high-quality data in near real-time, which is essential for seismic monitoring and alerting duties. Moreover, they improve seismicity maps, advance our understanding of seismotectonics, and enhance local seismic hazard assessments.

A noise analysis in the frequency domain revealed a split in the double-frequency microseisms at Balkan stations. This split is attributed to different source regions in the surrounding oceans. The shorter-period peak can likely be attributed to the generation in the nearby Ionian Sea, while a longer-period peak can be related to the distant North Atlantic and North Sea. This is also the generation area of the double-frequency peak at Central European stations. A seasonal variation of peak period and amplitude observed at all stations corresponds to seasonal meteorological effects. Stations located in sedimentary basins like the Pannonian Basin have the highest horizontal amplitudes in the DF microseisms.

The I95 amplitude values from a noise analysis in the time domain, along with corresponding violin and line plots, provide insights into the temporal variations of human activities at the sites.

The development of a PowBox, which monitors and controls the technical equipment of a station in cooperation with new monitoring software effectively reduces data gaps. This innovation is especially useful for installations in remote areas.

These advancements highlight the critical role of DSEBRA in contributing to large international arrays like AdriaArray. They underscore the importance of well-equipped station pools and international collaboration in achieving the scientific goals of large-scale seismic networks.

Field teams.

(1) Germany and Austria: M. Terpoorten (LMU), J. Loos (LMU), S. Egdorf (LMU)
(2) Hungary: T. Czifra (KRSO Budapest), B. Süle (KRSO Budapest)
(3) Kosovo: S. Mustafa, M. Terpoorten (LMU)
(4) Montenegro: M. Tomanovic, J. Dedic, M. Terpoorten (LMU)
(5) Albania: B. Rama (IGEO), M. Terpoorten (LMU)
(6) North Macedonia: D. Cernih (SORM), K. Drogreshka (SORM), J. Najdovska (SORM), Z. Todorov (SORM), J. Heuel (RUB), M. Paffrath (RUB)
(7) Greece: C. P. Evangelidis (NOA), I. Fountoulakis (NOA), K. Kontakos (NOA), S. Liakopoulos (NOA), G. Kaviris (NKUA), V. Kapetanidis (NKUA), V. Nikolis (NKUA), N. Sakellariou (NKUA), I. Spingos (NKUA), A. Zymvragakis (NKUA), E. Sokos (UPAT), N. Germenis (UPAT), C. Papazachos (AUTh), C. Ventouzi (AUTh), D. Vamvakaris (AUTh), N. Chatzis (AUTh), P. Paradisopoulou (AUTh), M. Ditz (RUB), K. Fischer (RUB), W. Friederich (RUB), A. Mohr(RUB).

Data availability statement. The code for the I95 toolbox is freely available on https://github.com/megies/i95_sds. The code for the SDS-monitoring software toolkit survBot is freely available on https://git.geophysik.ruhr-uni-bochum.de/marcel/survbot.

Acknowledgements. The authors thank the Deutsche Forschungsgemeinschaft (DFG) for funding DSEBRA (Deutsches Seismologisches Breitband Array) in the framework of the Priority Program SPP-2017 MB-4D (Mountain Building Processes in 4D) and for funding installation and maintenance of 60 stations within AdriaArray (WA1493/10-1, FR 1146/15-1). The authors are grateful to all members of the AdriaArray Seismology Group (Kolínský et al., 2025a).

References

Alder, C., E. Debayle, T. Bodin, A. Paul et al. (2021). Evidence for radial anisotropy in the lower crust of the Apennines from Bayesian ambient noise tomography in Europe, Geophys. J. Int., 226, 2, 941-967, doi:10.1093/gji/ggab066.

Ardhuin, F., L. Gualtieri and E. Stutzmann (2015). How ocean waves rock the Earth: Two mechanisms explain microseisms with periods 3 to 300 s, Geophys. Res. Lett., 42, 765-772, doi:10.1002/2014gl062782.

Bagagli, M., I. Molinari, T. Diehl and E. Kissling et al. (2025). Local earthquake tomography of the Alpine region from 24 years of data, Geophys. J. Int., 241, 1, 454-473, doi:10.1093/gji/ggaf028.

Beyreuther, M., R. Barsch, L. Krischer, T. Megies et al. (2010). ObsPy: A Python Toolbox for Seismology, Seismol. Res. Lett., 81(3), 530-533, doi:10.1785/gssrl.81.3.530.

Borzì, A. M., A. Cannata, F. Panzera, S. D'Amico et al. (2025). Microseism amplitude and wave power in the Mediterranean Sea (1996-2023), J. Geophys. Res. Solid Earth, 130, doi:10.1029/2024jb030528.

Bromirski, P. D., F. K. Duennebier and R. A. Stephen (2005). Mid-ocean microseisms, Geochem. Geophys. Geosyst., 6, doi:10.1029/2004gc000768.

Bromirski, P. D., R. A. Stephen and P. Gerstoft (2013). Are deep-ocean-generated surface-wave microseisms observed on land?, J. Geophys. Res. Solid Earth, 118, 3610-3629, doi:10.1002/jgrb.50268.

Caloiero, T., F. Aristodemo and D. A. Ferraro (2022). Annual and seasonal trend detection of significant wave height, energy period and wave power in the Mediterranean Sea, Ocean Eng., 243, 110322, doi:10.1016/j.oceaneng.2021.110322.

Cessaro, R. K. (1994). Sources of primary and secondary microseisms, Bull. Seismol. Soc. Am., 84, 142-148, doi:10.1785/bssa0840010142.

Dushi, E., B. Rama, A. Schlömer, S. Egdorf et al. (2025). AdriaArray in Albania: Collaborative Deployment, Station Characterization, and Data Integration, Ann. Geophys., submitted.

Evangelidis, C. P. and N. Melis (2012). Ambient noise levels in Greece as recorded at the Hellenic Unified Seismic Network, Bull. Seismol. Soc. Am., 102, 2507-2517, doi:10.1785/0120110319.

Evangelidis, C. P., N. Triantafyllis, M. Samios, K. Boukouras et al. (2021). Seismic waveform data from Greece and Cyprus: Integration, archival, and open access, Seismol. Res. Lett., 92, 1672-1684, doi:10.1785/0220200408.

Evangelidis, C. P. and I. Fountoulakis (2023). Imaging the Western Edge of the Aegean Shear Zone: The South Evia 2022-2023 Seismic Sequence, Seismica, 2, doi:10.26443/seismica.v2i1.1032.

Friederich, W., C. Evangelidis, C. Papazachos, E. Sokos et al. (2022). AdriaArray Temporary Network: Greece, North Macedonia, Data set, FDSN, doi:10.7914/y0t2-3b67.

Gráczer, Z., G. Szanyi, I. Bondár, C. Czanik et al. (2018). AlpArray in Hungary: temporary and permanent seismological networks in the transition zone between the Eastern Alps and the Pannonian basin, Acta Geod. Geophys., 53, 221-245, doi:10.1007/s40328-018-0213-4.

Groos, J. and J. Ritter (2009). Time domain classification and quantification of seismic noise in an urban environment, Geophys. J. Int., 179, 1213-1231, doi:10.1111/j.1365-246x.2009.04343.x.

Gualtieri, L., E. Stutzmann, C. Juretzek, C. Hadziioannou et al. (2019). Global scale analysis and modelling of primary microseisms, Geophys. J. Int., 218, 560-572, doi:10.1093/gji/ggz161.

Hasselmann, K. (1963). A statistical analysis of the generation of microseisms, Rev. Geophys., 1, 177-210, doi:10.1029/rg001i002p00177.

Heit, B., M. Weber, F. Tilmann, C. Haberland et al. (2017). The Swath-D Seismic Network in Italy and Austria, Data set, GFZ Data Services, doi:10.14470/MF7562601148.

Heit, B., L. Cristiano, C. Haberland, F. Tilmann et al. (2021). The SWATH-D seismological network in the Eastern Alps, Seismol. Res. Lett., 92, 1592-1609, doi:10.1785/0220200377.

Hetényi, G., I. Molinari, J. Clinton, G. Bokelmann et al. (2018). The AlpArray seismic network: a large-scale European experiment to image the Alpine Orogen, Surv. Geophys., 39, 1009-1033, doi:10.1007/s10712-018-9472-4.

Hetényi, G., J. Plomerová, M. Bielik, G. Bokelmann et al. (2019). Pannonian-Carpathian-Alpine seismic experiment, Data set, FDSN, doi:10.7914/SN/ZJ_2019.

Hunter, J. D. (2007). Matplotlib: A 2D graphics environment, Comput. Sci. Eng., 9, 90-95, doi:10.1109/mcse.2007.55.

Jha, K., P. B. Rao, C. Sribin and S. Silpa (2023). Analysis of seismic noise of broadband seismological stations installed along the Western Ghat, J. Seismol., 27, 325-342, doi:10.1007/s10950-023-10138-8.

Kalmár, D., L. Petrescu, J. Stipčević, A. Balázs et al. (2023). Lithospheric Structure of the Circum-Pannonian Region Imaged by S-To-P Receiver Functions, Geochem. Geophys. Geosyst., 24, 9, e2023GC010937, doi:10.1029/2023GC010937.

Kalmár, D., L. Petrescu, G. Hetényi, K. Michailos et al. (2025). Mantle transition zone analysis using P-to-S receiver functions in the Alpine-Carpathian-Dinarides region: impact of plumes and slabs, Geophys. J. Int., 243, 1, ggaf313, doi:10.1093/gji/ggaf313.

Kind, R., S. M. Schmid, X. Yuan, B. Heit et al. (2021). Moho and uppermost mantle structure in the Alpine area from S-to-P converted waves, Solid Earth, 12, 2503-2521, doi:10.5194/se-12-2503-2021.

Kind, R., S. M. Schmid, F. Schneider, T. Meier et al. (2023). Sp converted waves reveal the structure of the lithosphere below the Alps and their northern foreland, Geophys. J. Int., 235, 1832-1848, doi:10.1093/gji/ggad324.

Kolínský, P., G. Bokelmann and the AlpArray Working Group (2019). Arrival angles of teleseismic fundamental mode Rayleigh waves across the AlpArray, Geophys. J. Int., 218, 1, 115-144, doi:10.1093/gji/ggz081.

Kolínský, P., F. M. Schneider and G. Bokelmann (2020). Surface wave diffraction pattern recorded on AlpArray: Cameroon volcanic line case study, J. Geophys. Res. Solid Earth, 125, 7, e2019JB019102, doi:10.1029/2019JB019102.

Kolínský, P., T. Meier, M. Agius, A. Bijedić et al. (2025a). AdriaArray – a Passive Seismic Experiment to Study Structure, Geodynamics and Geohazards of the Adriatic Plate, Ann. Geophys., 68, doi:10.4401/ag-9284.

Kolínský, P., J. Stampa, L. Vecsey, F. Eickel et al. (2025b). Methods for data and metadata quality tests of large dense seismic networks – focus on AdriaArray, Ann. Geophys., submitted.

Koper, K. D. and R. Burlacu (2015). The fine structure of double-frequency microseisms recorded by seismometers in North America, J. Geophys. Res. Solid Earth, 120, 1677-1691, doi:10.1002/2014jb011820.

Krischer, L., T. Megies, R. Barsch, M. Beyreuther et al. (2015). ObsPy: A bridge for seismology into the scientific Python ecosystem, Comput. Sci. Discov., 8, 14003, doi:10.1088/1749-4699/8/1/014003.

Langston, C. A., S.-C. C. Chiu, Z. Lawrence, P. Bodin et al. (2009). Array observations of microseismic noise and the nature of H/V in the Mississippi embayment, Bull. Seismol. Soc. Am., 99, 2893-2911, doi:10.1785/0120080189.

Li, X., Y. Xu, C. Xie and S. Sun (2022). Global characteristics of ambient seismic noise, J. Seismol., 26, 343-358, doi:10.1007/s10950-021-10071-8.

Lu, Y., L. Stehly, A. Paul and AlpArray Working Group (2018). High-resolution surface wave tomography of the European crust and uppermost mantle from ambient seismic noise, Geophys. J. Int., 214, 2, 1136-1150, doi:10.1093/gji/ggy188.

Lu, Y., L. Stehly, R. Brossier, A. Paul et al. (2020). Imaging Alpine crust using ambient noise wave-equation tomography, Geophys. J. Int., 222, 1, 69-85, doi:10.1093/gji/ggaa145.

Lu, Y., H. A. Pedersen, L. Stehly and AlpArray Working Group (2022). Mapping the seismic noise field in Europe: spatio-temporal variations in wavefield composition and noise source contributions, Geophys. J. Int., 228, 1, 171-192, doi:10.1093/gji/ggab273.

Ling, O. K. A., S. C. Stähler, D. Giardini and the AlpArray Working Group (2021). Visualizing global seismic phases with AlpArray, Seismol. Soc. Am., 92, 6, 3845-3855, doi:10.1785/0220210046.

Longuet-Higgins, M. S. (1950). A theory of the origin of microseisms, Phil. Trans. R. Soc. Lond. A, 243, 1-35, doi:10.1098/rsta.1950.0012.

McNamara, D. E. and R. P. Buland (2004). Ambient noise levels in the continental United States, Bull. Seismol. Soc. Am., 94, 1517-1527, doi:10.1785/012003001.

Megies, T. (2024). I95 SDS (v0.1), Zenodo, doi:10.5281/zenodo.13987081.

Megies, T., M. Beyreuther, R. Barsch, L. Krischer et al. (2011). ObsPy – What can it do for data centers and observatories?, Ann. Geophys., 54, 47-58, doi:10.4401/ag-4838.

Menichelli, I., P. De Gori, F. P. Lucente, L. Improta et al. (2023). Lithosphere structure, processes, and physical state of the Alpine-Apennine System, J. Geophys. Res. Solid Earth, 128, e2023JB026411, doi:10.1029/2023JB026411.

Michailos, K., G. Hetényi, M. Scarponi, J. Stipčević et al. (2022). Moho depths beneath the European Alps: a homogeneously processed map and receiver functions database, Earth Syst. Sci. Data, 15, 2117-2138, doi:10.5194/essd-15-2117-2023.

Mroczek, S., F. Tilmann, J. Pleuger, X. Yuan et al. (2023). Investigating the Eastern Alpine-Dinaric transition with teleseismic receiver functions: Evidence for subducted European crust, Earth Planet. Sci. Lett., 609, 118096, doi:10.1016/j.epsl.2023.118096.

Najafabadi, J. A., C. Haberland, E. Le Breton, M. R. Handy et al. (2022). Constraints on crustal structure in the vicinity of the Adriatic Indenter (European Alps) from Vp and Vp/Vs local earthquake tomography, J. Geophys. Res. Solid Earth, 127, e2021JB023160, doi:10.1029/2021JB023160.

Nouibat, A., R. Brossier, L. Stehly, J. Cao et al. (2023). Ambient-noise wave-equation tomography of the Alps and Ligurian-Provence Basin, J. Geophys. Res. Solid Earth, 128, e2023JB026776, doi:10.1029/2023JB026776.

Paffrath, M., W. Friederich and the AlpArray and AlpArray-SWATH D Working Groups (2021a). Teleseismic P waves at the AlpArray seismic network: wave fronts, absolute travel times and travel-time residuals, Solid Earth, 12, 7, 1635-1660, doi:10.5194/se-12-1635-2021.

Paffrath, M., W. Friederich, S. M. Schmid, M. R. Handy et al. (2021b). Imaging structure and geometry of slabs in the greater Alpine area – a P-wave travel-time tomography using AlpArray Seismic Network data, Solid Earth, 12, 2671-2702, doi:10.5194/se-12-2671-2021.

Peterson, J. R. (1993). Observations and Modeling of Seismic Background Noise, US Geol. Surv., doi:10.3133/ofr93322.

Plomerová, J., H. Žlebčíková, G. Hetényi, L. Vecsey et al. (2022). Two subduction-related heterogeneities beneath the Eastern Alps and the Bohemian Massif imaged by high-resolution P-wave tomography, Solid Earth, 13, 251-270, doi:10.5194/se-13-251-2022.

Retailleau, L., P. Boué, L. Stehly and M. Campillo (2017). Locating microseism sources using spurious arrivals in intercontinental noise correlations, J. Geophys. Res. Solid Earth, 122, 8107-8120 doi:10.1002/2017jb014593.

Rykunov, L. (1967). Microseisms. Experimental characteristics of natural ground microvibrations in the period range of 0.07-8 s, Nauka, Moscow.

Sartini, L., G. Besio and F. Cassola (2017). Spatio-temporal modelling of extreme wave heights in the Mediterranean Sea, Ocean Model., 117, 52-69, doi:10.1016/j.ocemod.2017.07.001.

Schlömer, A., J. Wassermann, W. Friederich, M. Korn et al. (2022a). UNIBRA/DSEBRA: The German Seismological Broadband Array and Its Contribution to AlpArray – Deployment and Performance, Seismol. Res. Lett., 93, 2077-2095, doi:10.1785/0220210287.

Schlömer, A., J. Wassermann, J. Plomerová, L. Vecsey et al. (2022b). AdriaArray Temporary Network: Albania, Austria, Czech Rep., Germany, Hungary, Kosovo, Montenegro, Slovakia, Data set, FDSN, doi:10.7914/2cat-tq59.

Schlömer, A., G. Hetényi, J. Plomerová, L. Vecsey et al. (2024). The Pannonian-Carpathian-Alpine seismic experiment (PACASE): network description and implementation, Acta Geod. Geophys., 1-22, doi:10.1007/s40328-024-00439-w.

Seismological Observatory at the Faculty of Natural Sciences and Mathematics, Ss. Cyril and Methodius University, Skopje, Republic of Macedonia (1966). Seismological network of the Republic of North Macedonia, Data set, FSDN, doi:10.7914/v6tz-xh04.

Spingos, I., G. Kaviris, V. Kapetanidis, E. Papadimitriou et al. (2024). Shear-wave splitting associated with fluid processes beneath Styra, South Euboea: First results, Phys. Earth Planet. Inter., 351, 107196, doi:10.1016/j.pepi.2024.107196.

Stampa, J., F. Eckel and T. Meier (2025). Visualizing wavefields with AdriaArray, Ann. Geophys., 68, doi:10.4401/ag-9329.

Strollo, A., D. Cambaz, J. Clinton, P. Danecek et al. (2021). EIDA: The European integrated data archive and service infrastructure within ORFEUS, Seismol. Res. Lett., 92, 1788-1795, doi:10.1785/0220200413.

Stutzmann, E., M. Schimmel, G. Patau and A. Maggi (2009). Global climate imprint on seismic noise, Geochem. Geophys. Geosyst., 10, Q11004, doi:10.1029/2009GC002619.

Süle, B., B. Czecze, T. Czifra, M. Csatlós et al. (2025). Seismological Network in Hungary: Insights from the AdriaArray Operational Period, Ann. Geophys., 68, doi:10.4401/ag-9321.

Tesch, M., J. Stampa, T. Meier, E. Kissling et al. (2022). Imaging seismic wave-fields with AlpArray and neighboring European networks, Int. J. Earth Sci., 111, 1, 321-334, doi:10.1007/s00531-021-02116-7.

Timkó, M., A. El-Sharkawy, L. Wiesenberg, L. Fodor et al. (2024). Crustal and upper mantle 3-D Vs structure of the Pannonian region from joint earthquake and ambient noise Rayleigh wave tomography, Geophys. J. Int., 239, 1313-1334, doi:10.1093/gji/ggae314.

Triantafyllis, N., I. E. Venetis, I. Fountoulakis, E.-V. Pikoulis et al. (2021). Gisola: A high-performance computing application for real-time moment tensor inversion, Seismol. Res. Lett., 93, 957-966, doi:10.1785/0220210153.

University of Athens (2008). Hellenic Seismological Network, University of Athens, Seismological Laboratory, Data set, FDSN, doi:10.7914/SN/HA.

Waskom, M. L. (2021). seaborn: statistical data visualization, J. Open Source Softw., 6, 3021, doi:10.21105/joss.03021.

Wiesenberg, L., C. Weidle, K. Krämer, C. Pilger et al. (2024). Seismic monitoring of the October 2023 storm surge along the coast of the Baltic Sea, Die Küste 94, Bundesanstalt für Wasserbau, doi:10.18171/1.094104.

Zürn, W., J. Exß, H. Steffen, C. Kroner et al. (2007). On reduction of long-period horizontal seismic noise using local barometric pressure, Geophys. J. Int., 171, 780-796, doi:10.1111/j.1365-246x.2007.03553.x.

Appendix A.

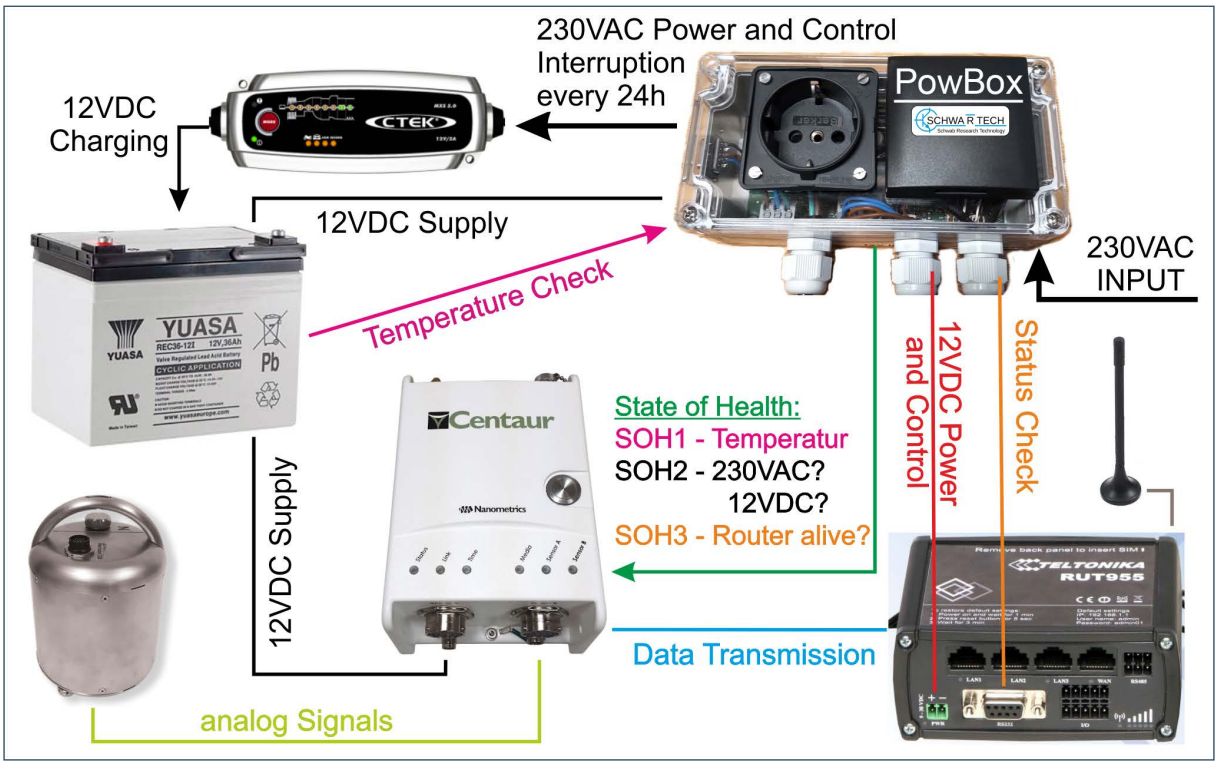

Figure A1. Circuit diagram of the PowBox (upper right) implemented in the technical equipment of a DSEBRA station.

Appendix B.

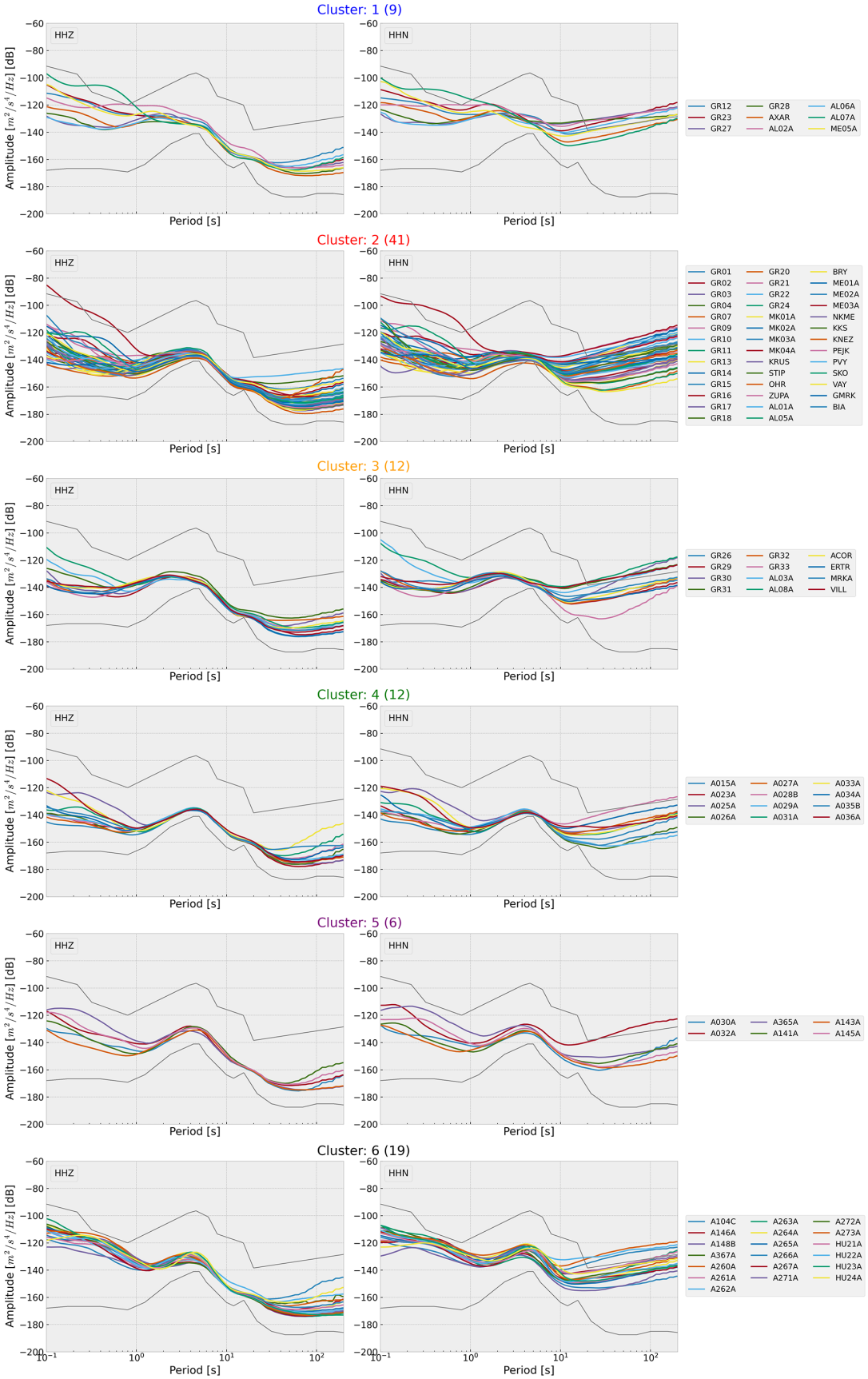

Figure B1. Mean Probabilistic Power Spectral Densities (PPSDs) for the summer season (01 June–31 August 2023) of all DSEBRA and RUB stations, assigned to six different noise clusters.

Appendix C.

The management of I95 noise levels is handled by a slim Python toolbox called “I95 SDS”, developed at LMU (Megies, 2024). The primary ideas are to maintain a simple workflow, process data in real time to assess noise levels during acquisition and minimize storage requirements for the processed data.

The toolbox consists of two main components. Firstly, a Python script that calculates and stores I95 noise levels, and secondly, a Python module that provides high-level routines for visualizing the previously computed noise values.

The processing script can be executed from the command line to compute I95 noise levels based on daily raw waveform data stored in a local SeisComP Data Structure (SDS) archive. The calculated noise levels are efficiently stored in NumPy’s “npy” format and organized within the SDS structure for convenient retrieval and visualization. Typically, processing is automated via cron jobs on a Linux server, running daily. However, it can also be started manually when reprocessing is required, e.g., when data from offline stations is retrospectively added to the archive. Noise level processing is straightforward and utilizes the ObsPy framework (Beyreuther et al., 2010; Megies et al., 2011; Krischer et al., 2015). Continuous waveforms are segmented into shorter time windows with buffer regions at the start and end that are trimmed after preprocessing. The instrument response is removed, and the data is demeaned and filtered within a predefined frequency range. An I95 noise value is then calculated for each window and stored – together with its timestamp – with the other time windows for the same channel and day in a single file. All processing parameters are pre-configured and stored in a simple JSON file located in the root directory of the noise level SDS archive.

The visualization module relies on Matplotlib (Hunter, 2007) and seaborn (Waskom, 2021) packages. It provides an intuitive high-level Python class “I95SDSClient”, which allows users to generate plots for any channel or time range of the precomputed SDS noise data archive. The data can be visualized in a condensed manner, showing the statistical distribution of I95 noise values as a violin plot, as a temporal evolution of noise levels as a wiggle plot, or in a color-coded image plot.

More details are available on the project’s GitHub page (https://github.com/megies/i95_sds).

Appendix D.

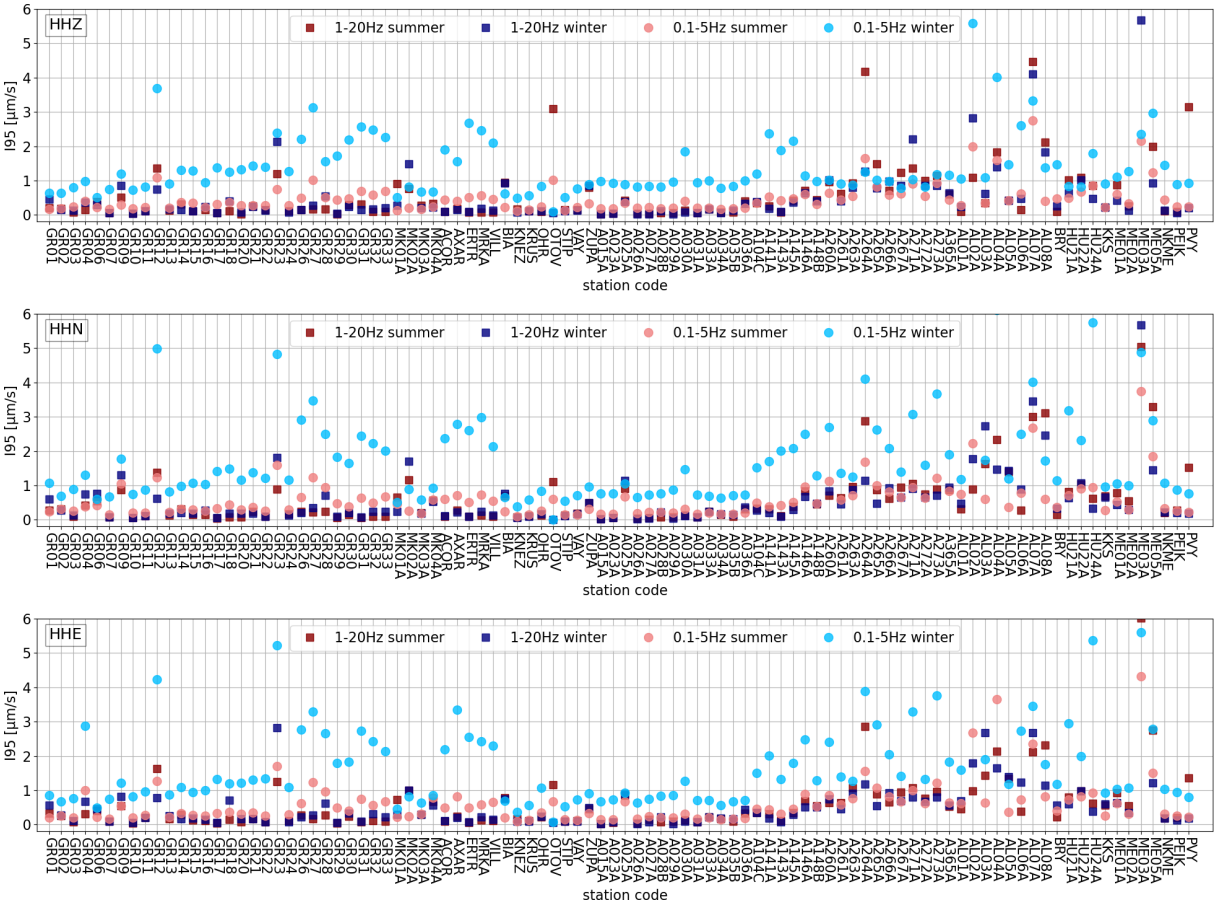

Figure D1. Comparison of I95 amplitude values calculated in two different frequency ranges (0.1-5 Hz: circles and 1-20 Hz: squares) during summer (warm colors) and winter (cold colors) for all components.

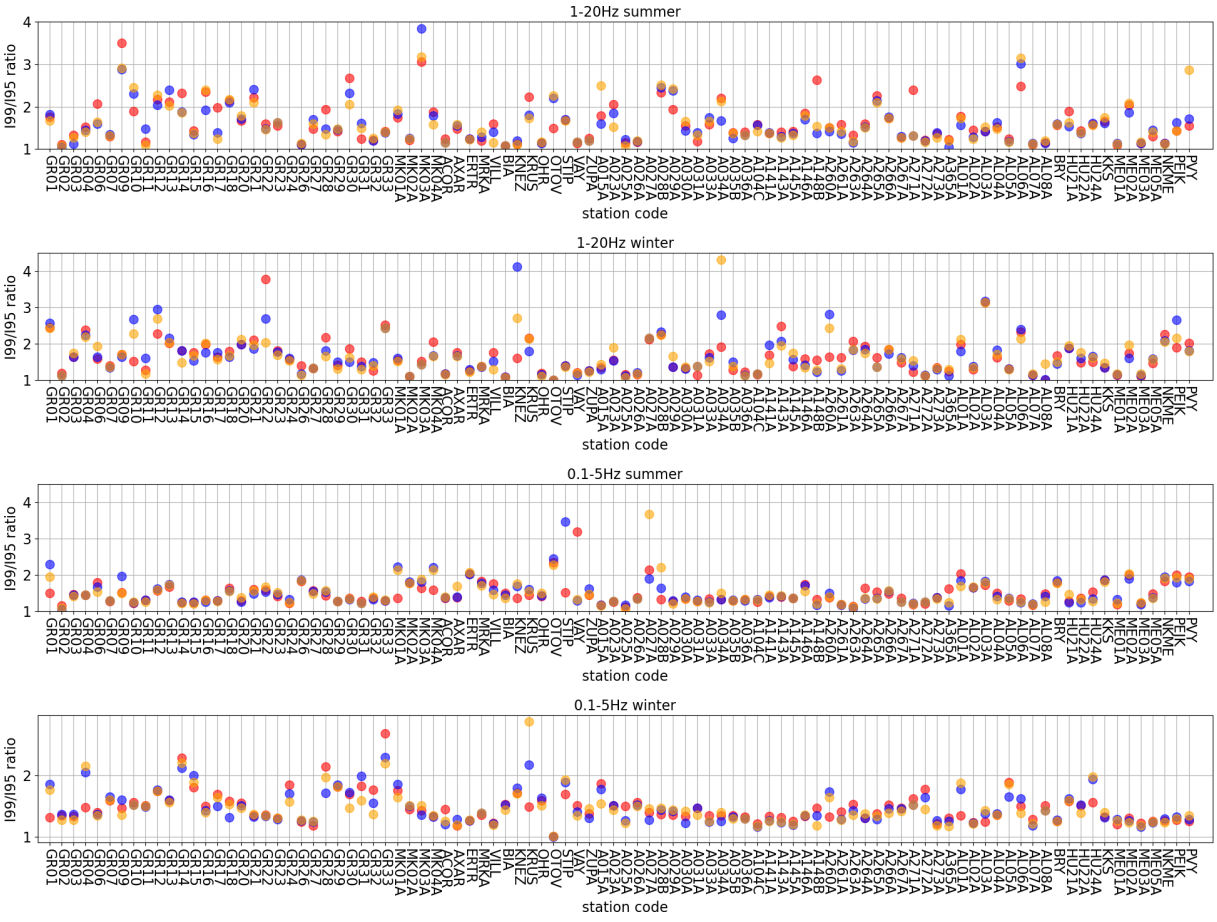

Figure D2. I99/I95 ratios calculated in two different frequency ranges during summer and winter for all components.

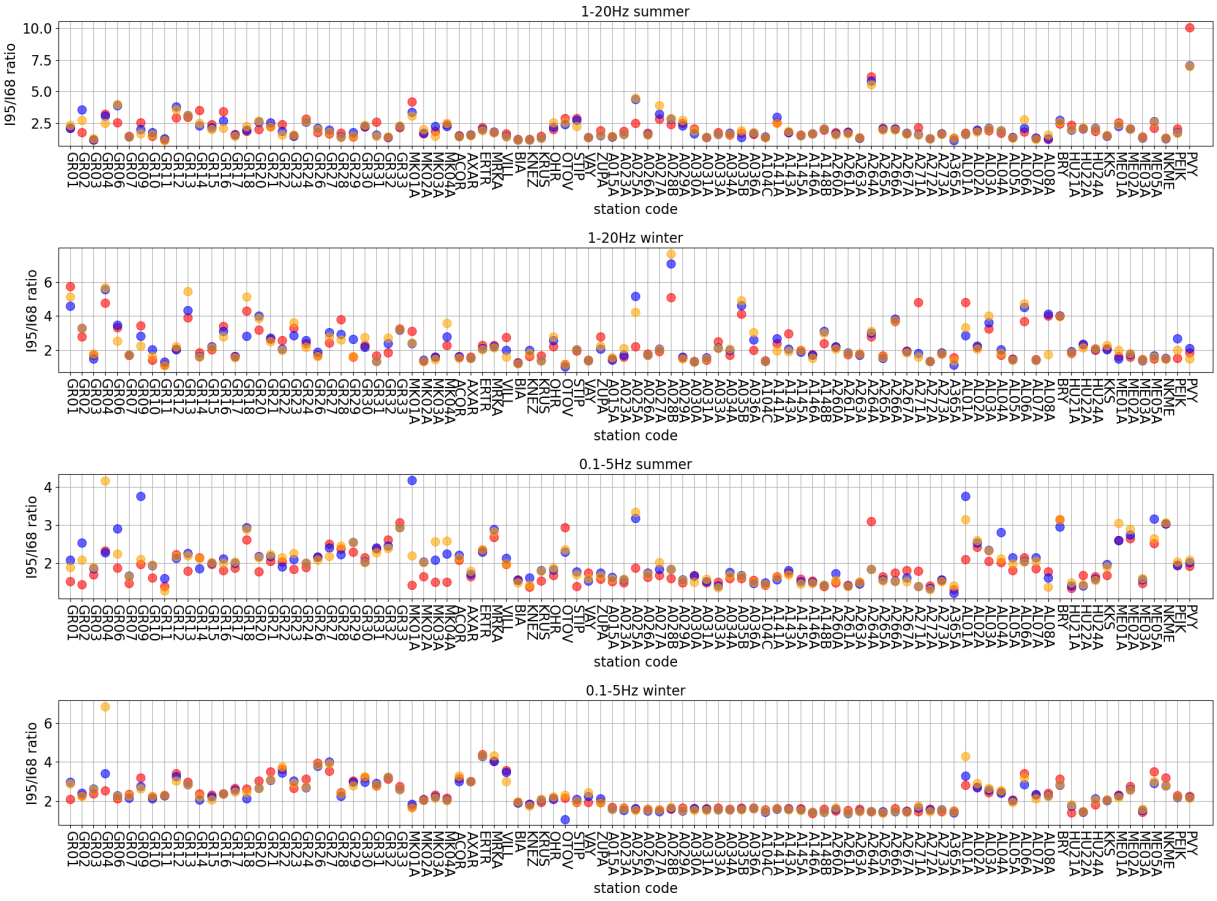

Figure D3. I95/I68 ratios calculated in two different frequency ranges during summer and winter for all components.

***CORRESPONDING AUTHOR: Antje SCHLÖMER**,
Ludwig-Maximilians-Universität München, Department of Earth and Environmental Sciences, 80333 Munich, Germany
e-mail: Antje.Schloemer@lmu.de